

Electronic Supplementary Information

Interaction of Synthetic and Lignin-based Sulfonated Polymers with Hydrophilic, Hydrophobic, and Charged Self-Assembled Monolayers

Armin Eraghi Kazzaz and Pedram Fatehi*

Biorefining Research Institute, Green Processes Research Centre and Chemical Engineering
Department, Lakehead University, 955 Oliver Road, Thunder Bay, ON, Canada, P7B5E1

* Corresponding author

Supporting methods

Gel Permeation Chromatography (GPC)

In this set of experiments, 40 mg of pretreated (under different pH) PVA-A and L-S samples were dissolved in 10 mL of 0.1 mol/L of NaNO₃ solution and filtered using a 0.2 μm nylon filter and used for molecular weight analysis. The eluent of the system was 0.1 M sodium nitrate solution with a flow rate of 0.7 mL/min in the GPC. The refractometer (RI) and differential pressure (DP) detectors were used to determine the molecular weight of the samples. All measurements were conducted with respect to standard polyethylene oxide.

Phenolic hydroxyl and carboxylate group analysis

The phenolic hydroxyl and carboxylate group contents were determined according to eq. 1 and eq. 2, respectively:

$$\text{Phenolic hydroxyl group (mmol/g)} = \frac{((EP'_2 - EP'_1) - (EP_2 - EP_1)) \times C}{m} \quad (1)$$

$$\text{Carboxylate group (mmol/g)} = \frac{((EP'_3 - EP'_2) - (EP_3 - EP_2)) \times C}{m} \quad (2)$$

where C is the concentration of HCl (mol/L) as a titrant, m is the dried weight of the polymer used in the analysis. EP'_1 , EP'_2 , and EP'_3 are the used volumes of HCl solution (mL) at the first, second, and third end points when the S-L sample was titrated. EP_1 , EP_2 , and EP_3 are the consumed volumes of HCl solution (mL) at the first, second, and third end points, respectively, when titrating the control sample (blank solution).

¹H NMR and FTIR spectroscopy

In this experiment, 1 mg of TMSP and 25-40 mg of the samples were dissolved in 500 μL of D₂O or [D₆]DMSO for 12 h at 50 °C in a water bath shaker at 150 rpm.^{1,2}

The FTIR experiment was carried out by using ~0.1 g of freeze-dried polymer samples. Then, 32 scans of each sample with a 4 cm⁻¹ resolution and the spectra range of 700 to 4000 cm⁻¹ were recorded.

Quartz crystal microbalance with dissipation (QCM-D)

Senses were cleaned by using the following procedure. The gold sensors were cleaned with a mixture of 1:1:5 of H₂O₂ (30%): NH₃ (25%): Milli-Q water for 7 min at 60 °C, rinsed with Milli-Q water and then dried nitrogen gas. The sensors were further cleaned by UV/ozone (digital UV ozone system, PSD Series, NOVASCAN) and treated for 10 min. Hereafter, they were rinsed with Milli-Q water and dried with nitrogen gas.

The adsorbed wet mass per unit based on the Sauerbrey model is calculated following eq. (3):

$$\Delta m_{\text{sauerbrey}} = -\frac{C\Delta f}{n} \quad (3)$$

where Δm and Δf are adsorbed mass and frequency changes, respectively. C is a constant value (0.177 mg/m² Hz for 5 MHz AT-cut quartz crystal sensor), n is the measurement overtone used.

Supporting results

¹H NMR spectroscopy

In Figure S1, the peak at 7.42-5.99 ppm is attributed to the aromatic protons, the peak at 4.5-3.05 and 3.6-3.2 ppm are ascribed to the methoxy group protons of lignin's, and methylene protons in the β-β structure, respectively. The peaks appearing at 4.7, and 0.0 ppm are assigned to D₂O, and TMSP (3-trimethylsilyl-(2,2,3,3-D₄)-propionic acid sodium salt), respectively.²⁻⁴ In Figure S2, the peaks at 2.52, and 3.5 ppm are associated with [D₆]DMSO and H₂O.⁵

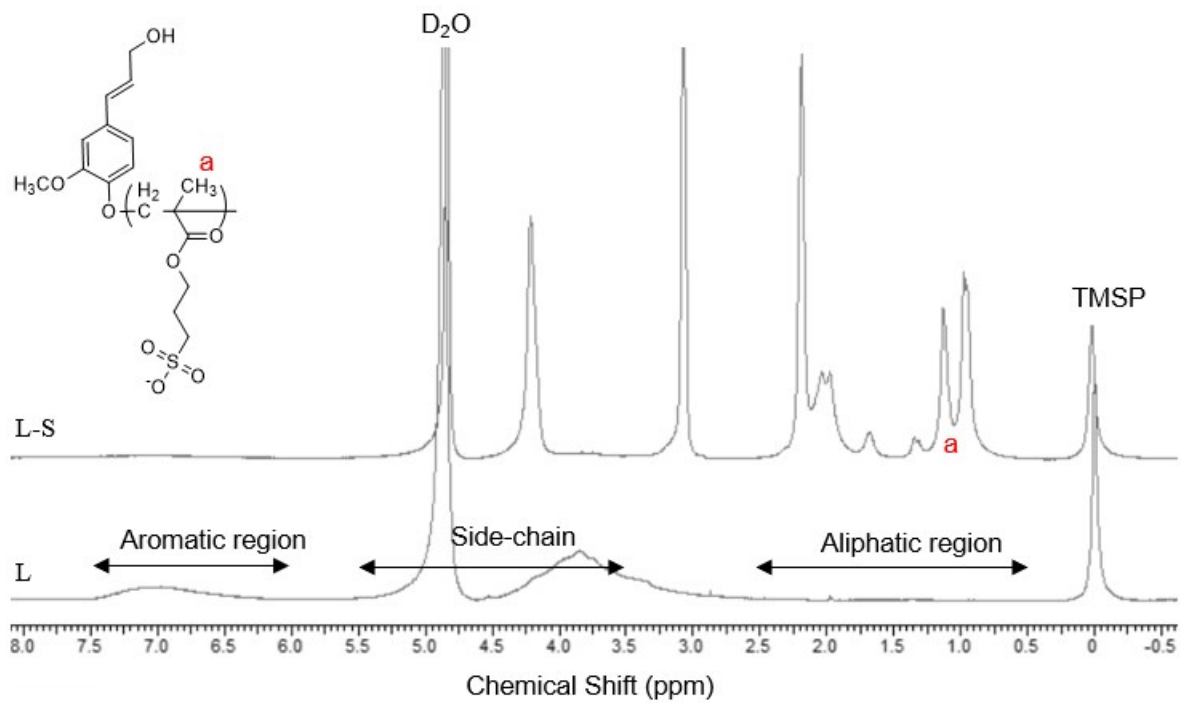


Figure S1. ^1H NMR spectrum of L, and L-S in D_2O , at 25°C .

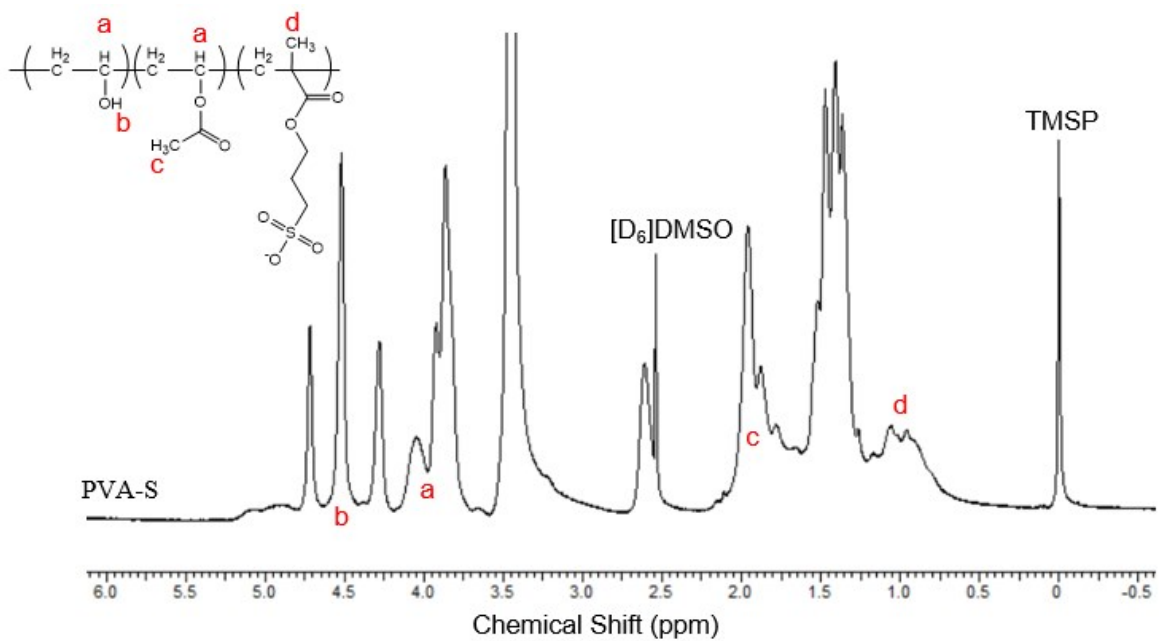


Figure S2. ^1H NMR spectrum PVA-S in $[\text{D}_6]\text{DMSO}$, at 25°C .

FTIR Spectroscopy

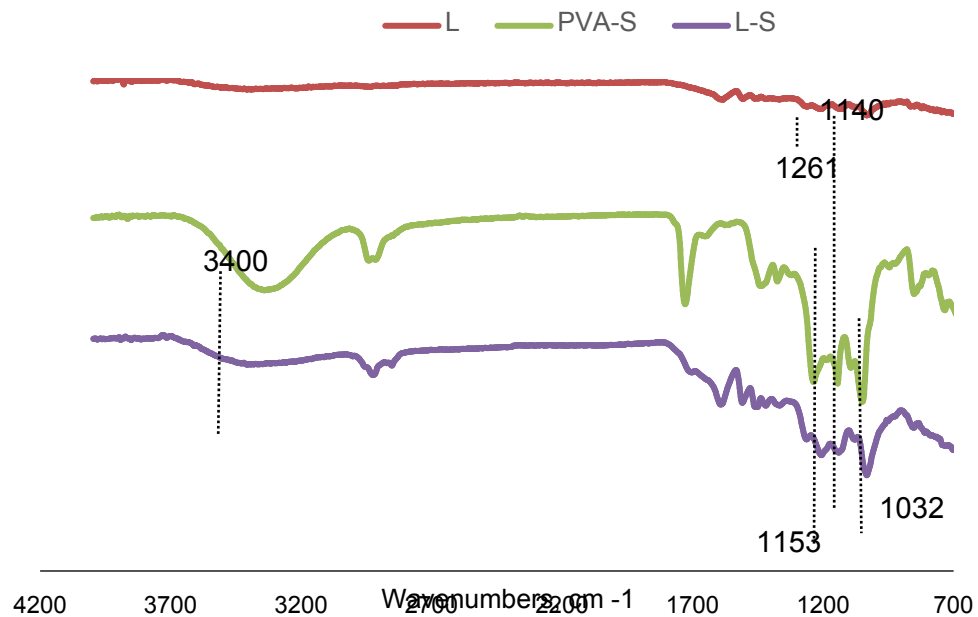


Figure S3. FTIR spectra of L, PVA-S, and L-S samples, at 25 °C.

Table S1. Assignment of the adsorption in FTIR spectra.

Entry	Band position (cm ⁻¹)	Assignment	References
1	1261	The C-O stretch of guaiacyl unit	2,6,7
2	1140	The C-H stretch of guaiacyl unit	2,7,8
3	3400	O-H stretching absorption in the phenolic and aliphatic parts of lignin	6
4	1032	C-O-C bond illustrating the ether linkages between the polymer and anionic monomer	6,9
5	1140+-20	The S=O stretch of the sulfonate group	10,11
6	1750-1711	C=O stretch of ester	1,5

Gel permeation chromatography (GPC)

Table S2. PVA-S, and L-S molecular weight analysis by GPC after incubation for 12 h and dialysis.

pH	PVA-S molecular weight (g/mol)	L-S molecular weight (g/mol)
4.0	104,500	111,200
6.7	113,100	114,700
11.0	103,000	114,500

Zeta potential analysis

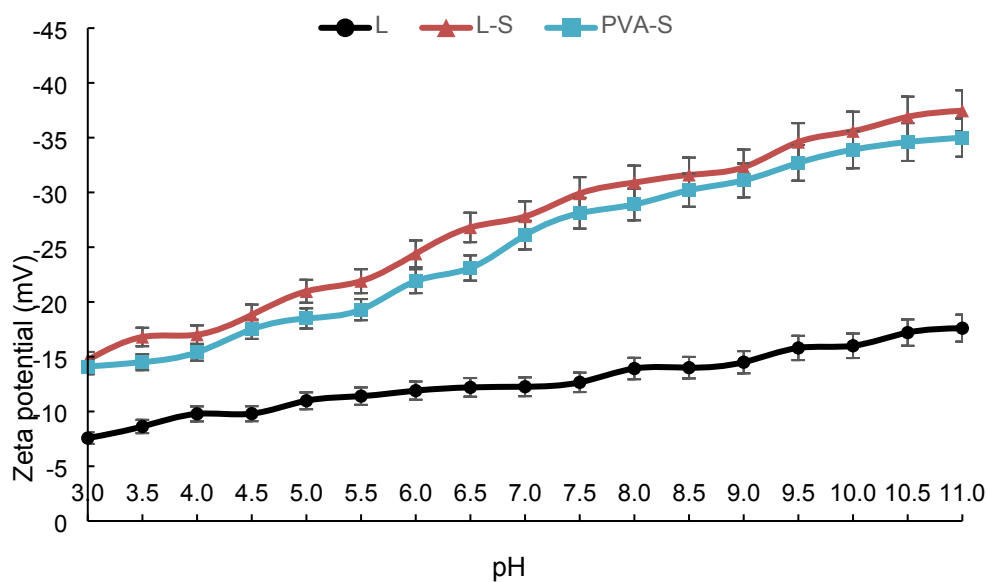


Figure S4. The zeta potential analysis of L, L-S, and PVA-S samples under different pH at 25 °C.

X-ray photoelectron spectroscopy (XPS)

Table S3. Surface composition of the SAM-terminated surfaces.

Chemical formula	SAMs name	Atomic percentage (at.%)			
		N	C	O	S
HS(CH ₂) ₁₁ OH	11-mercapto-1-undecanol	-	82.6	13.1	4.3
HS(CH ₂) ₁₁ COOH	12-mercaptododecanoic acid	-	78.4	18.5	3.1
HS(CH ₂) ₁₁ CH ₃	1-dodecanethiol	-	91.6	3.8	4.6
HS(CH ₂) ₆ NH ₂ HCl	6-amino-1-hexanethiol hydrochloride	5.6	78.7	11.1	4.6

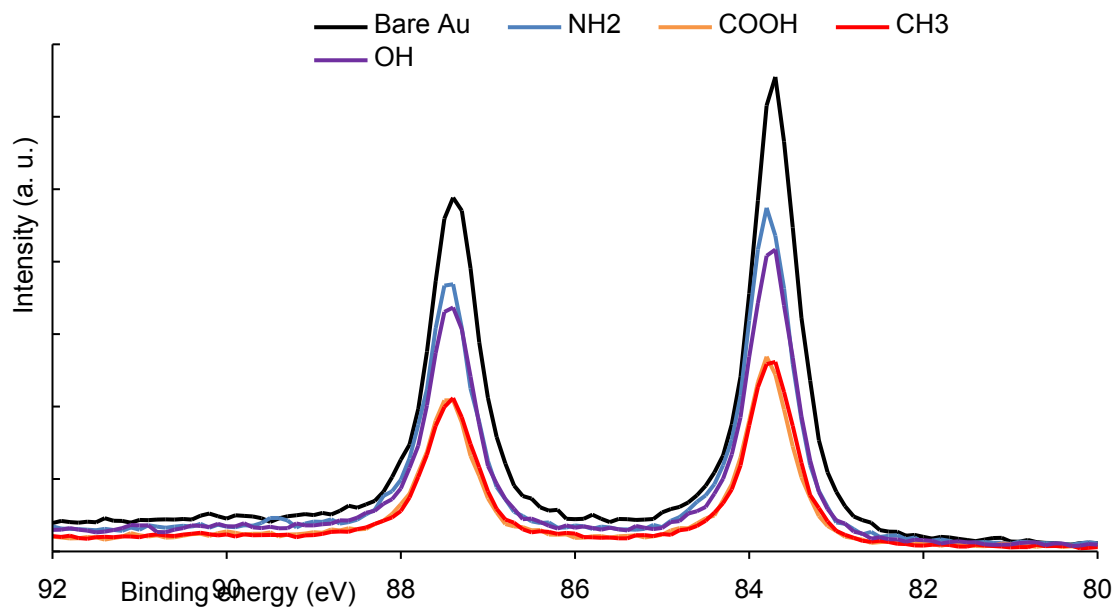


Figure S5. XPS high-resolution spectra in the Au4f region for a bare gold (as reference), and different terminated SAMs on Au.

Water adsorption at a different temperature on different SAM surfaces

Adsorption on -OH-functionalized surface

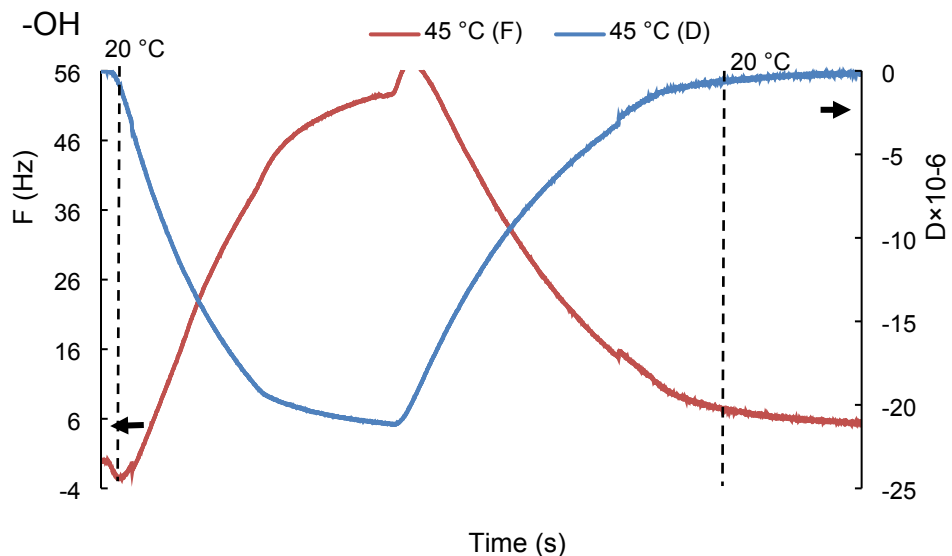


Figure S6. Frequency and dissipation changes of the 9th overtone of water adsorption on the -OH-functionalized surface at different temperatures.

Adsorption on -COOH-functionalized surface

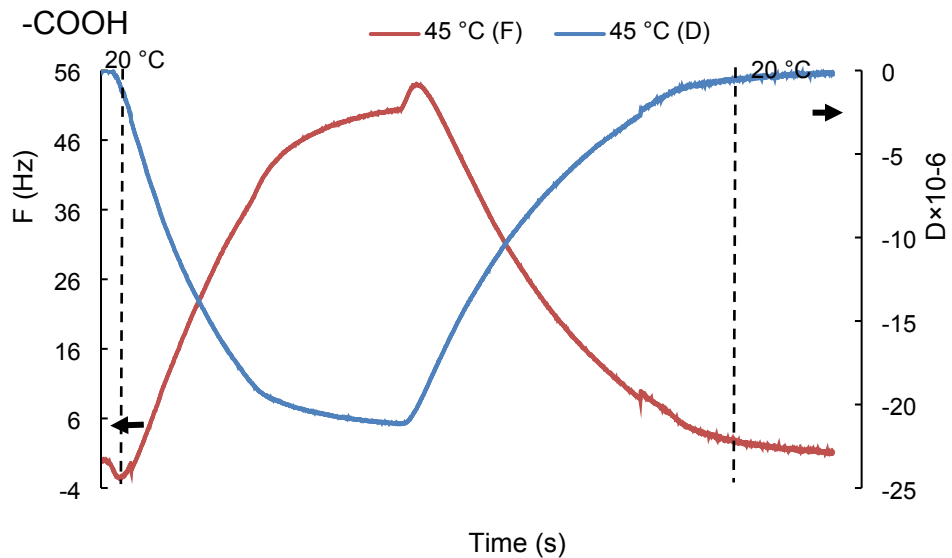


Figure S7. Frequency and dissipation changes of the 9th overtone of water adsorption on the -COOH-functionalized surface at different temperatures.

Adsorption on -CH₃-functionalized surface

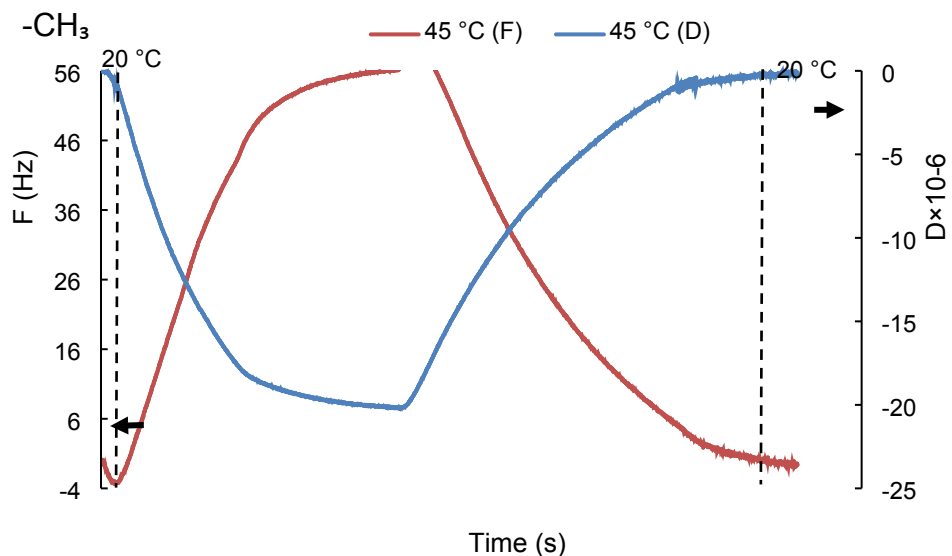


Figure S8. Frequency and dissipation changes of the 9th overtone of water adsorption on the -CH₃-functionalized surface at different temperatures.

Adsorption on -NH₂-functionalized surface

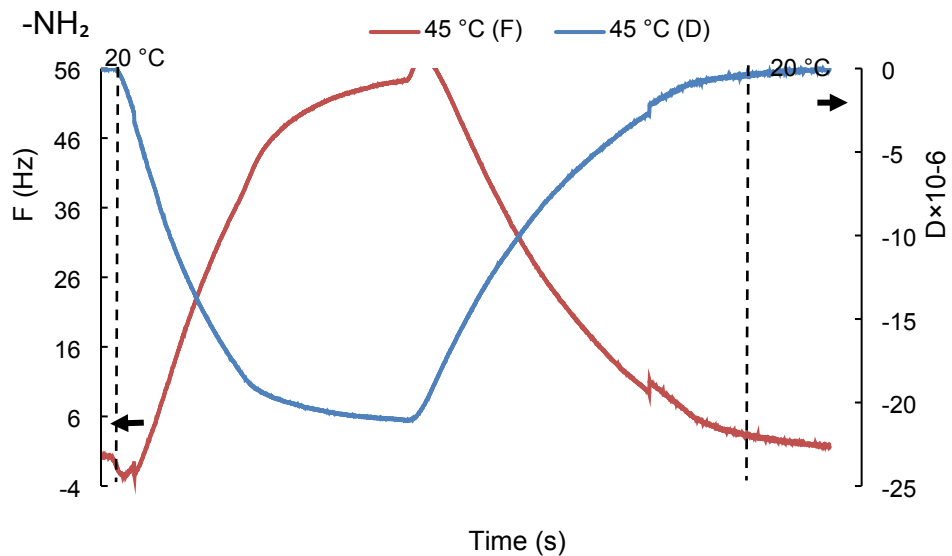


Figure S9. Frequency and dissipation changes of the 9th overtone of water adsorption on the -NH₂-functionalized surface at different temperatures.

Water adsorption at different pH on different SAM surfaces

Adsorption on -OH-functionalized surface

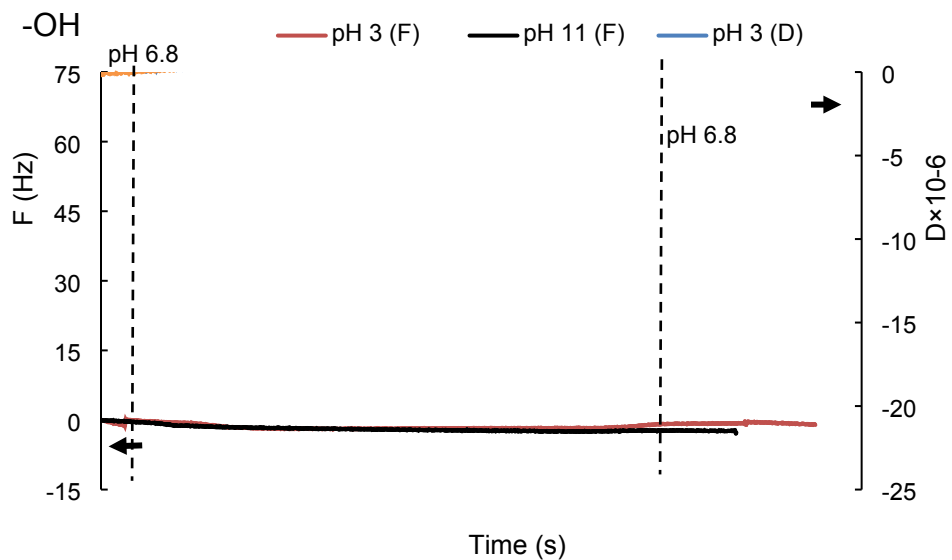


Figure S10. Frequency and dissipation changes of the 9th overtone of water adsorption on the -OH-functionalized surface at pH.

Adsorption on -COOH-functionalized surface

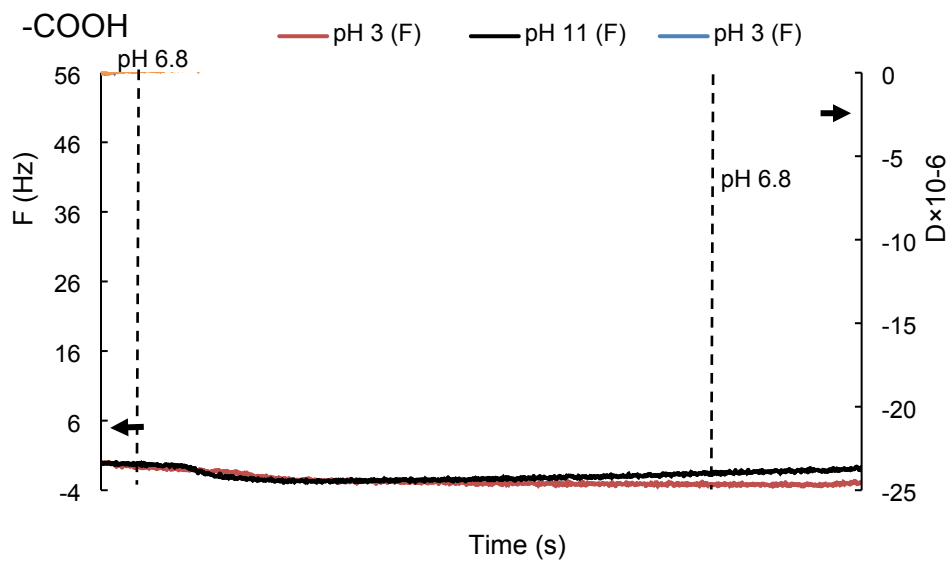


Figure S11. Frequency and dissipation changes of the 9th overtone of water adsorption on the -COOH-functionalized surface at pH.

Adsorption on -CH₃-functionalized surface

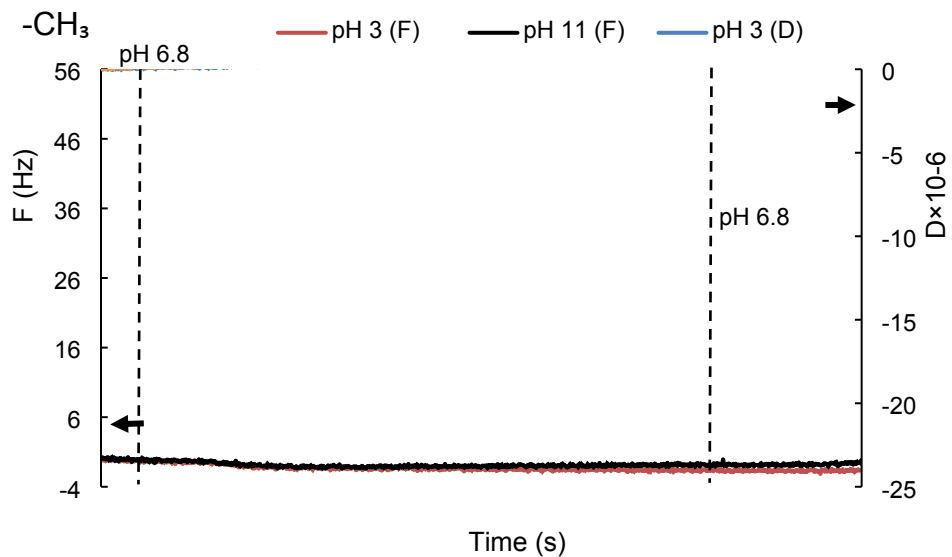


Figure S12. Frequency and dissipation changes of the 9th overtone of water adsorption on the -CH₃-functionalized surface at pH.

Adsorption on -NH₂-functionalized surface

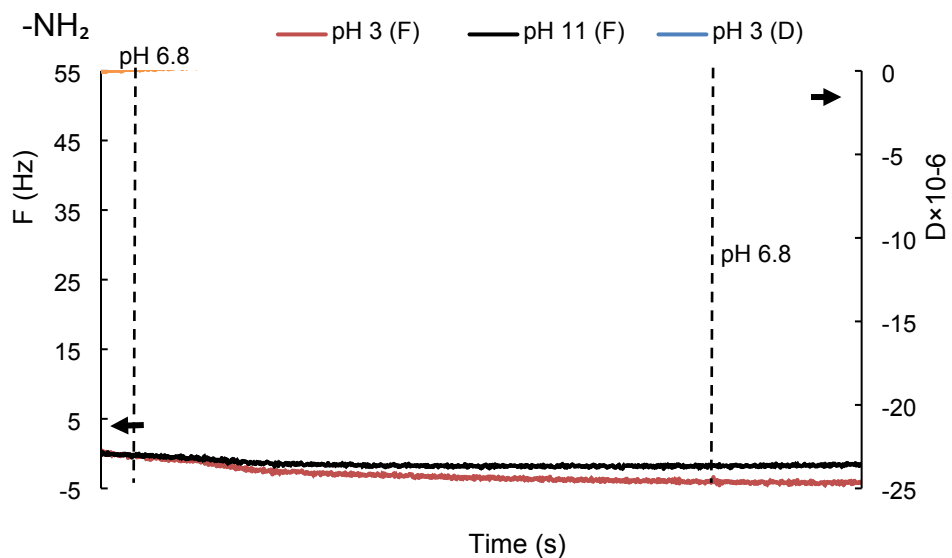


Figure S13. Frequency and dissipation changes of the 9th overtone of water adsorption on the -NH₂-functionalized surface at pH.

Effect of temperature on the adsorption of L-S, and PVA-S on SAMs

Adsorption on -OH-functionalized surface

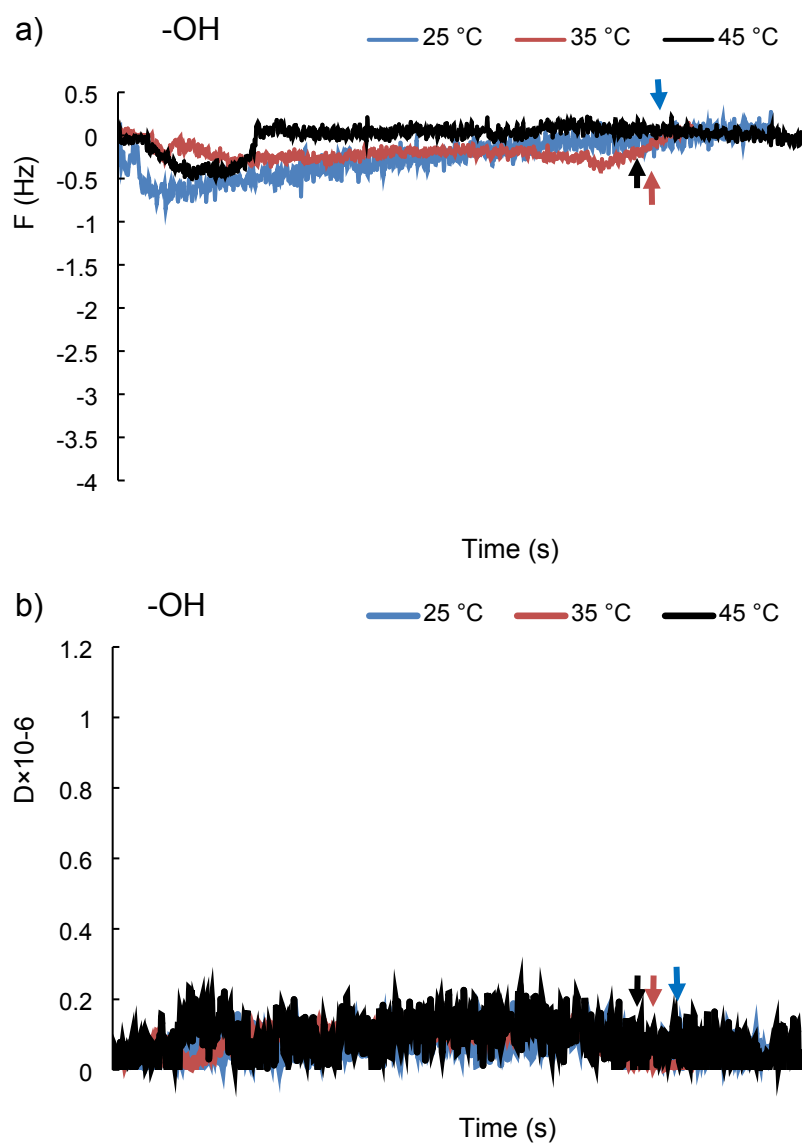


Figure S14. a) frequency b) dissipation changes of the 9th overtone of the adsorption of L-S polymer on the -OH-functionalized surface at different temperatures (arrows indicate buffer rinsing).

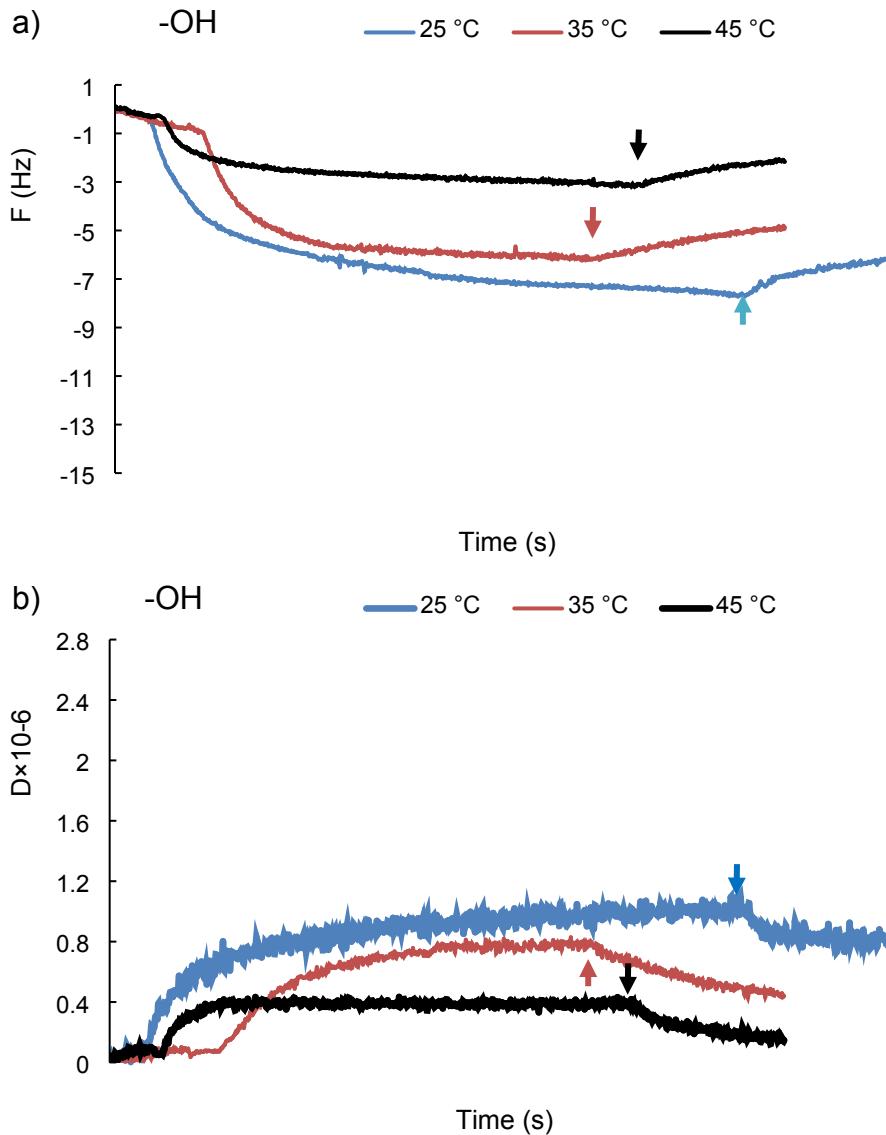


Figure S15. a) frequency b) dissipation changes of the 9th overtone of the adsorption of PVA-S polymer on the -OH-functionalized surface at different temperatures (arrows indicate buffer rinsing).

Adsorption on -COOH-functionalized surface

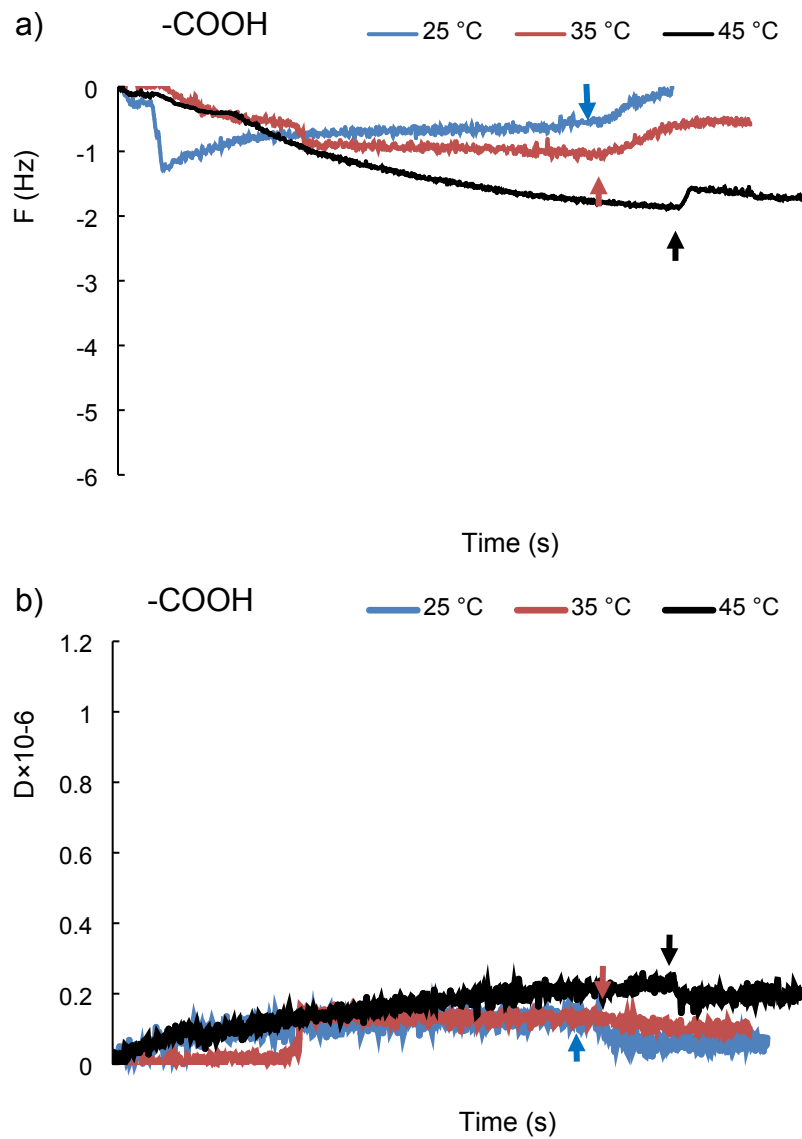


Figure S16. a) frequency b) dissipation changes of the 9th overtone of the adsorption of L-S polymer on the -COOH-functionalized surface at different temperatures (arrows indicate buffer rinsing).

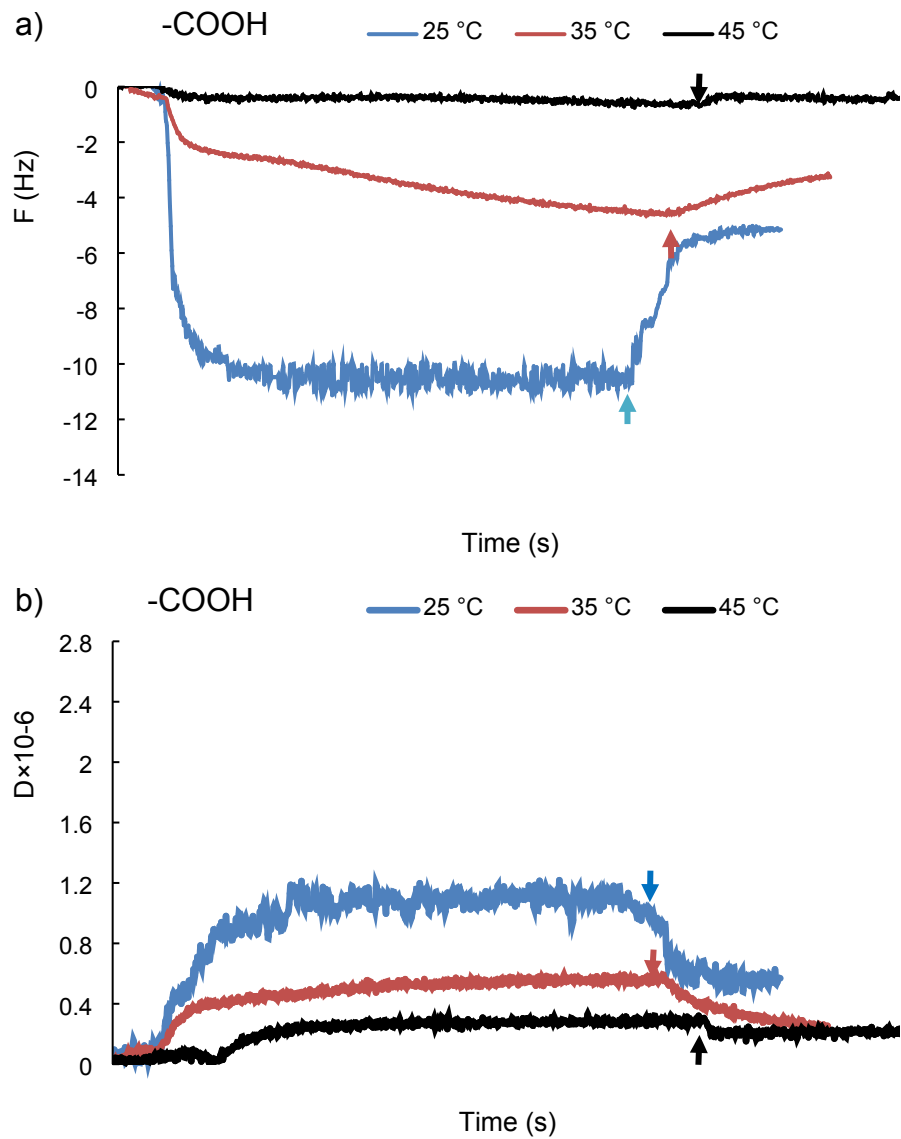


Figure S17. a) frequency b) dissipation changes of the 9th overtone of the adsorption of PVA-S polymer on the -COOH-functionalized surface at different temperatures (arrows indicate buffer rinsing).

Adsorption on -CH₃-functionalized surface

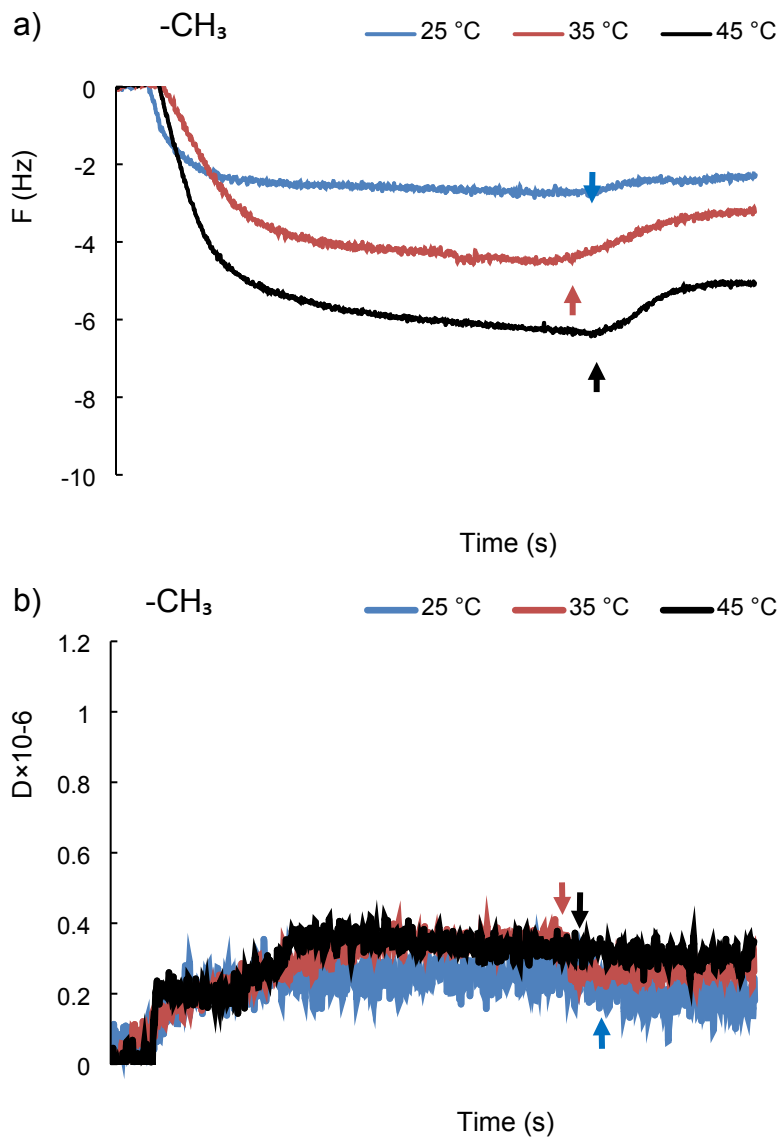


Figure S18. a) frequency b) dissipation changes of the 9th overtone of the adsorption of L-S polymer on the $-\text{CH}_3$ -functionalized surface at different temperatures (arrows indicate buffer rinsing).

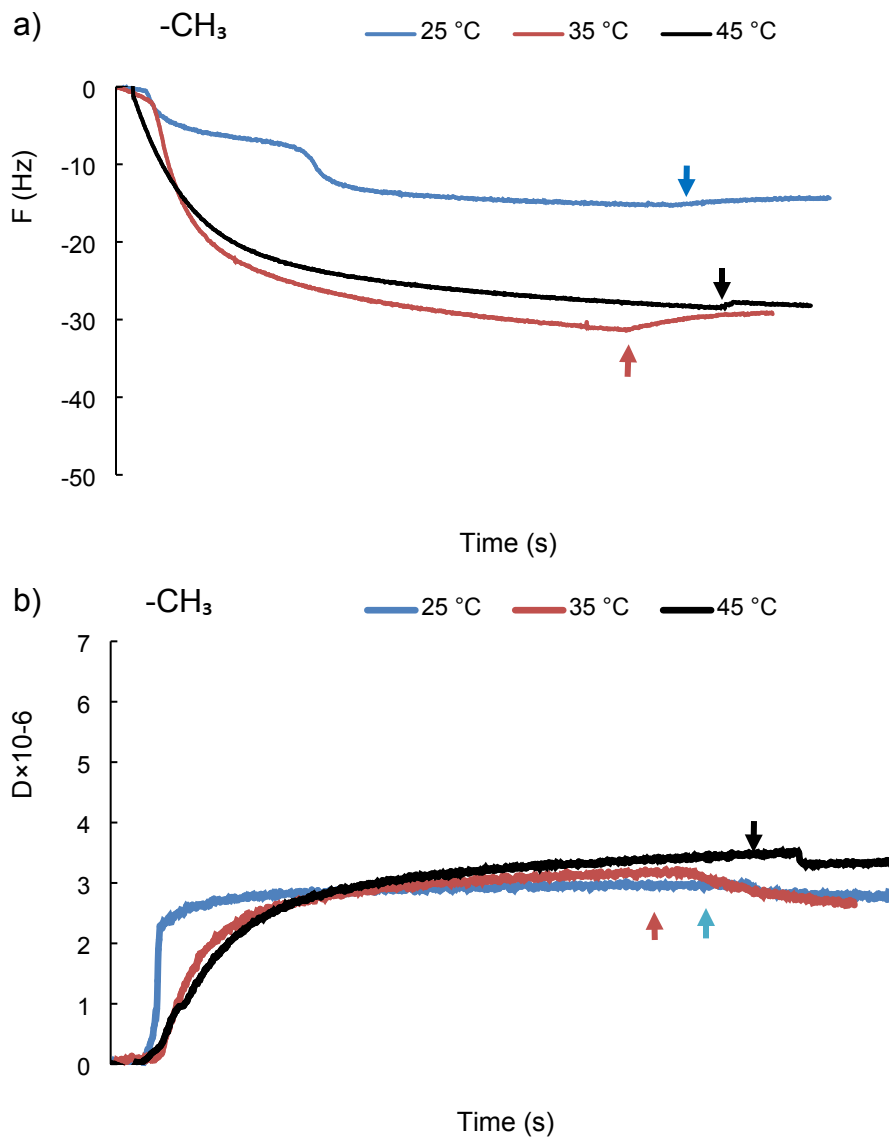


Figure S19. a) frequency b) dissipation changes of the 9th overtone of the adsorption of PVA-S polymer on the $-\text{CH}_3$ -functionalized surface at different temperatures (arrows indicate buffer rinsing).

Adsorption on $-\text{NH}_2$ -functionalized surface

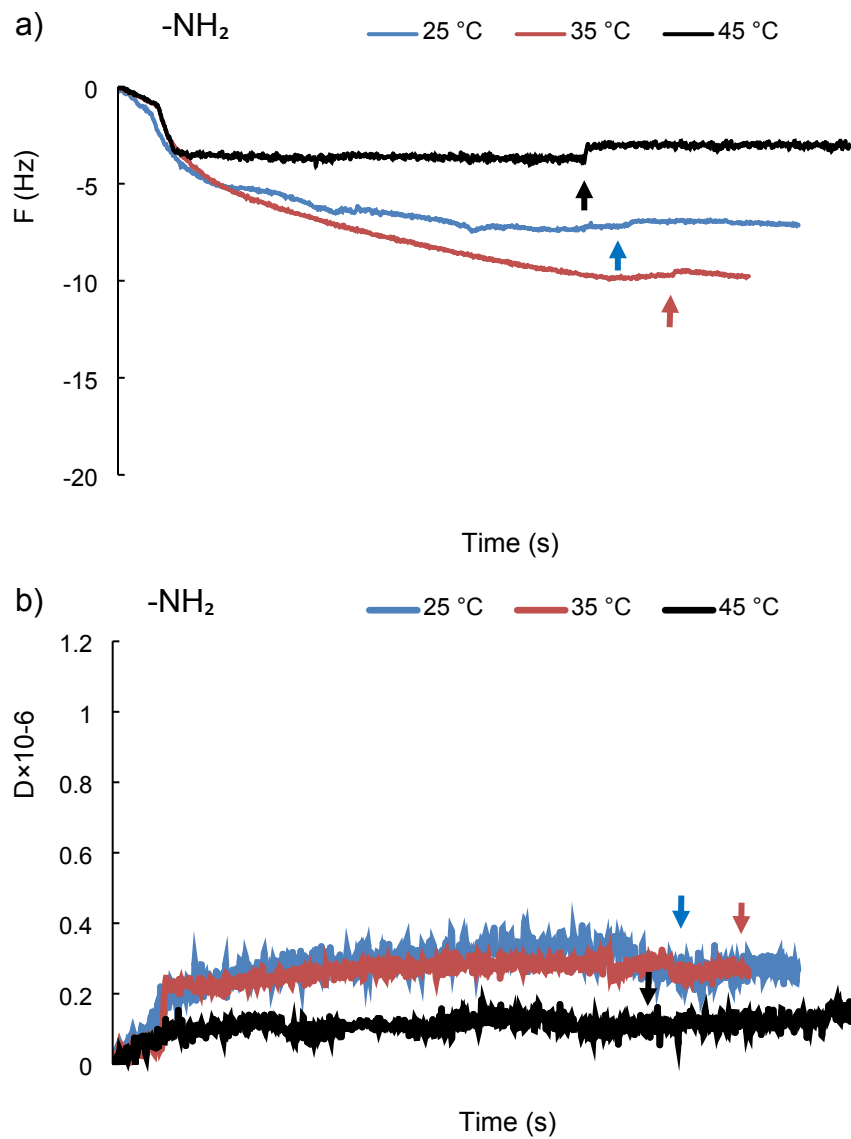


Figure S20. a) frequency b) dissipation changes of the 9th overtone of the adsorption of L-S polymer on the $-\text{NH}_2$ -functionalized surface at different temperatures (arrows indicate buffer rinsing).

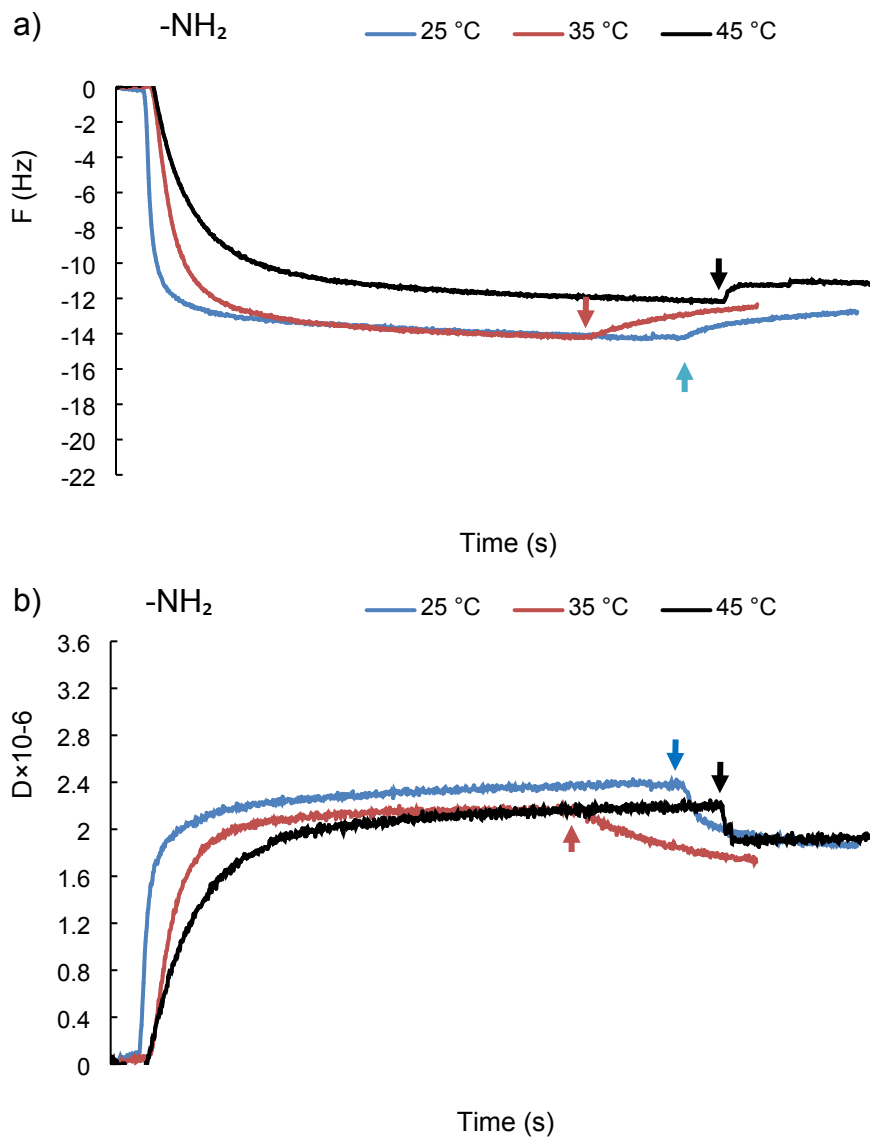


Figure S21. a) frequency b) dissipation changes of the 9th overtone of the adsorption of PVA-S polymer on the -NH₂-functionalized surface at different temperatures (arrows indicate buffer rinsing).

Effect of pH on the adsorption of L-S, and PVA-S on SAMs

Adsorption on -OH-functionalized surface

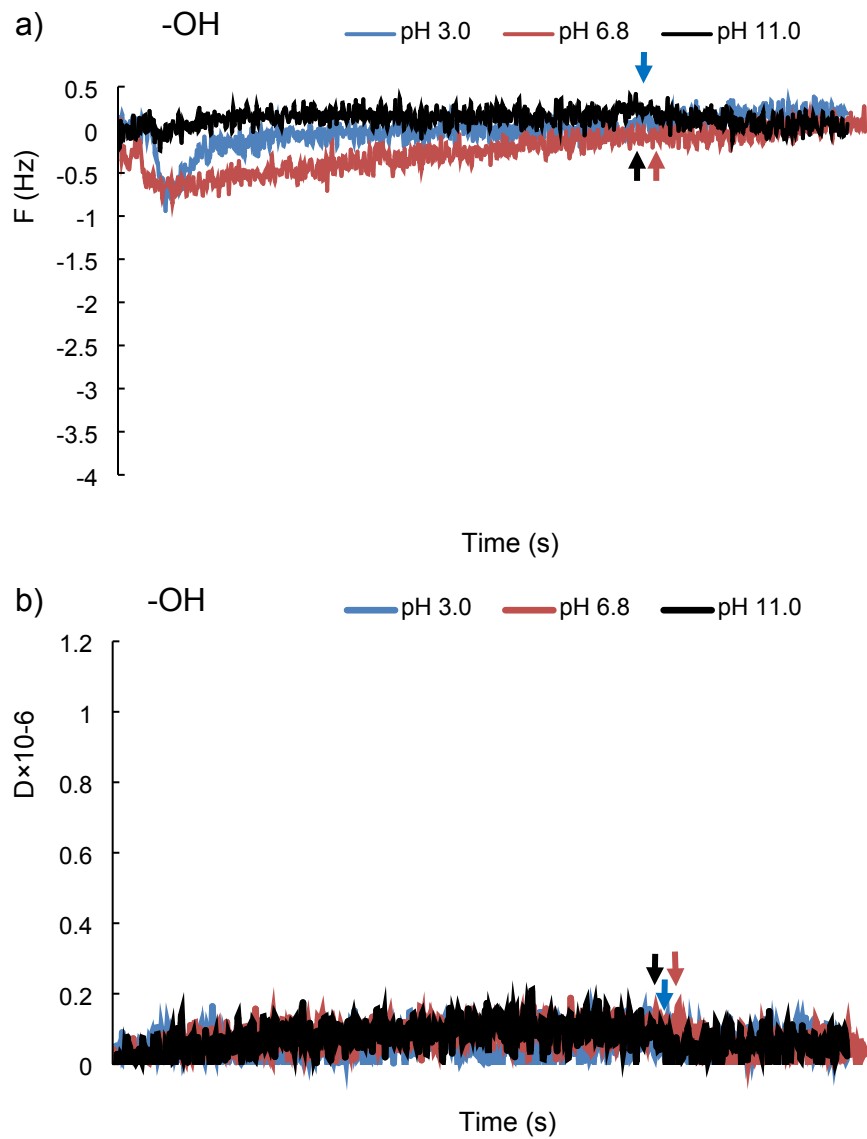


Figure S22. a) frequency b) dissipation changes of the 9th overtone of the adsorption of L-S polymer on the -OH-functionalized surface at different pH (arrows indicate buffer rinsing).

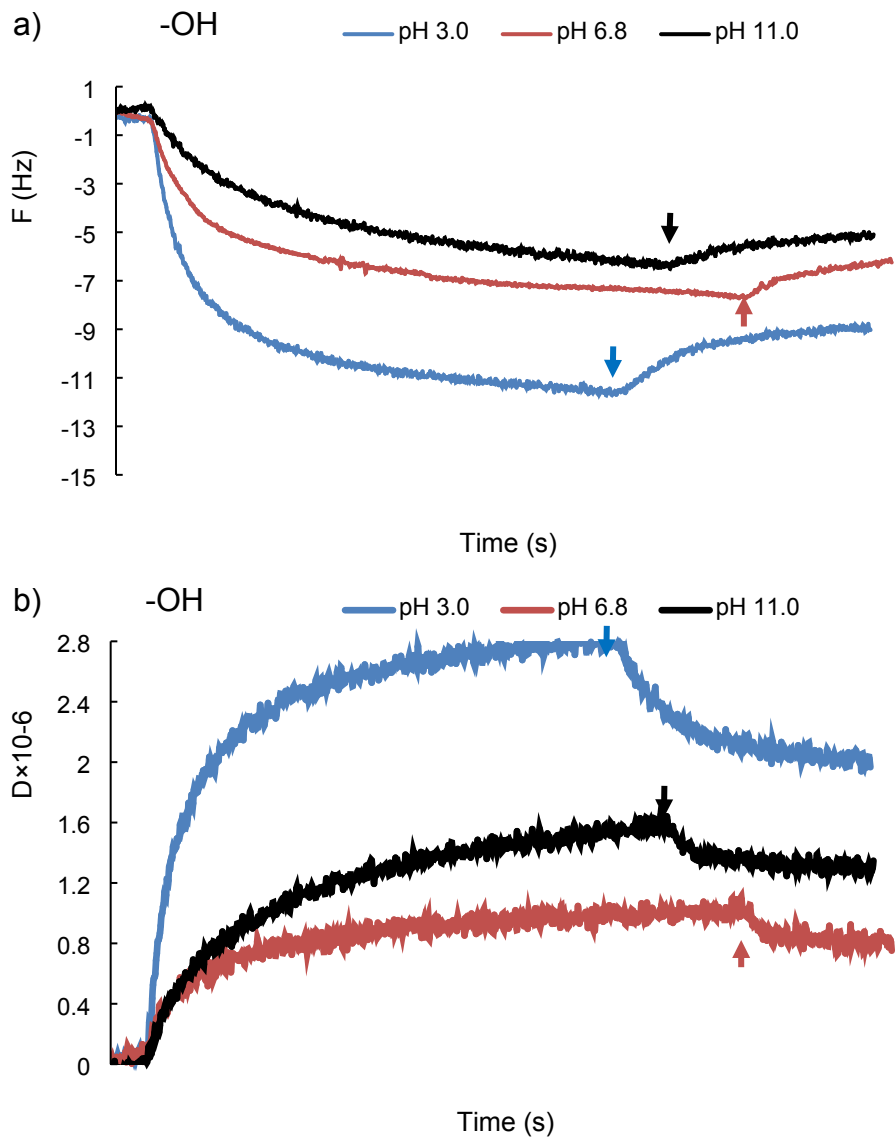


Figure S23. a) frequency b) dissipation changes of the 9th overtone of the adsorption of PVA-S polymer on the -OH-functionalized surface at different pH (arrows indicate buffer rinsing).

Table S4. Contact angle of water-air ($\theta_{W/A}$) interfaces of PVA-S, and L-S polymers at different pH.

pH	PVA-S	L-S
3.0	11°±0.5	38°±0.5

6.7	$12^{\circ} \pm 1$	$17^{\circ} \pm 1$
11.0	$10^{\circ} \pm 1$	$15^{\circ} \pm 0.5$

Adsorption on -COOH-functionalized surface

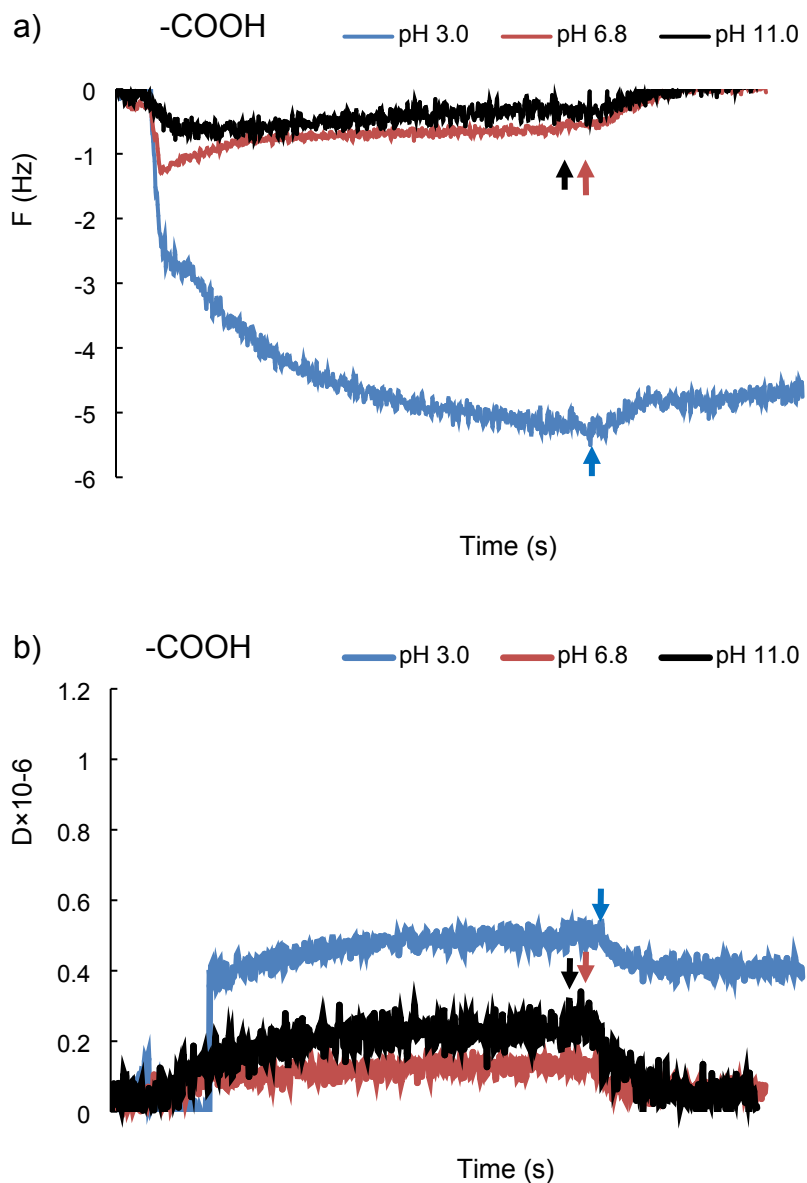


Figure S24. a) frequency b) dissipation changes of the 9th overtone of the adsorption of L-S polymer on the -COOH-functionalized surface at different pH (arrows indicate buffer rinsing).

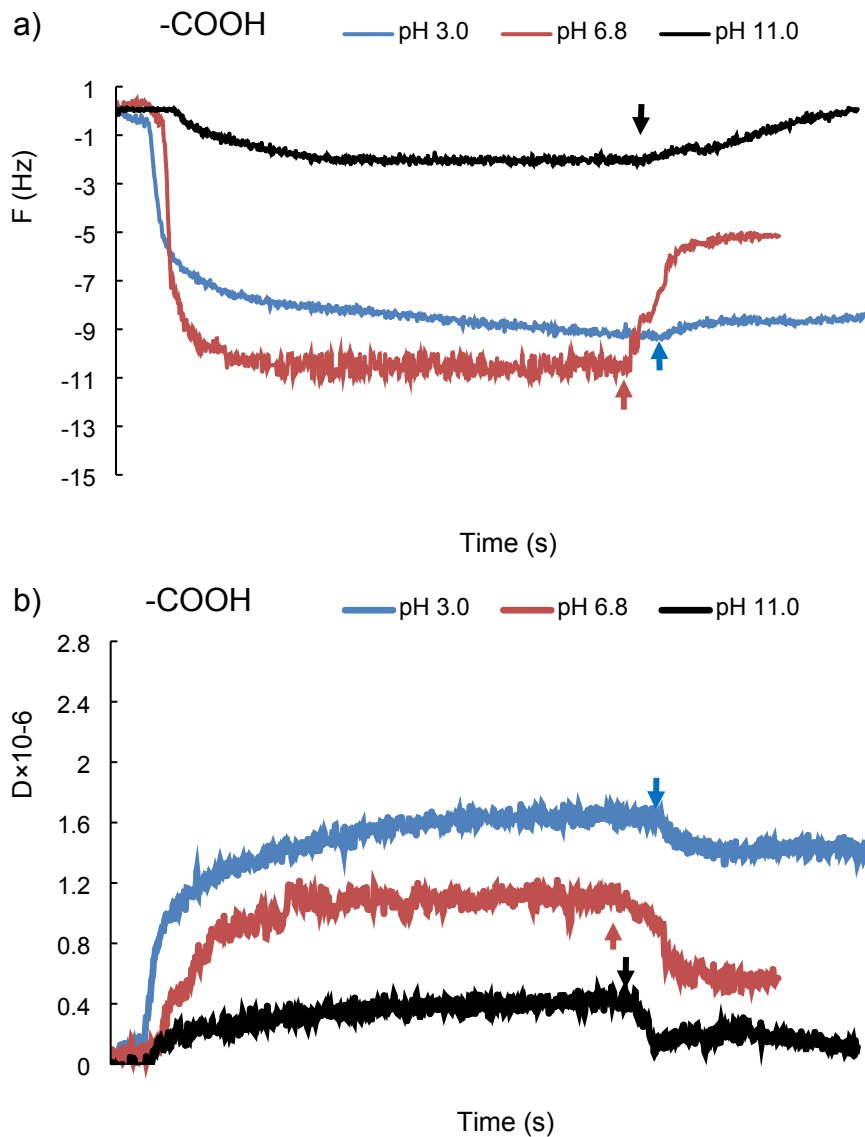


Figure S25. a) frequency b) dissipation changes of the 9th overtone of the adsorption of PVA-S polymer on the -COOH-functionalized surface at different pH (arrows indicate buffer rinsing).

Adsorption on -CH₃-functionalized surface

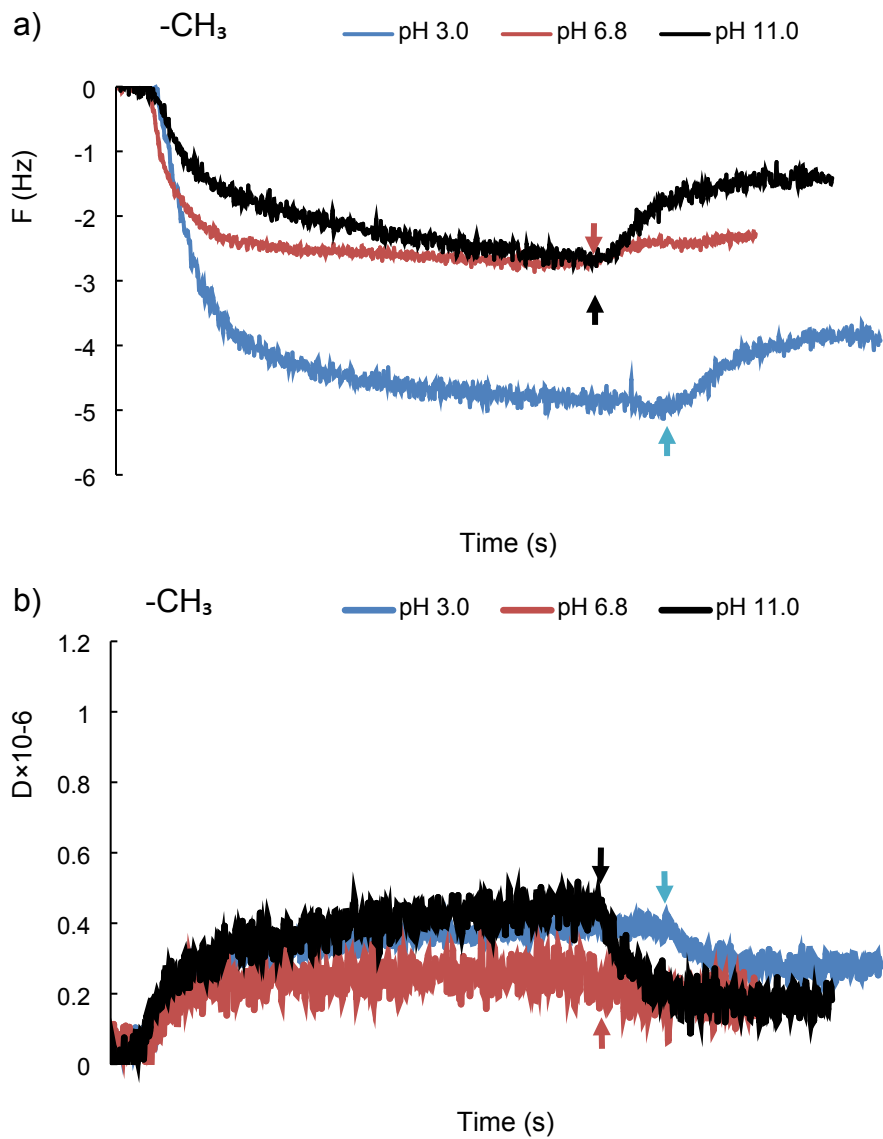


Figure S26. a) frequency b) dissipation changes of the 9th overtone of the adsorption of L-S polymer on the $-\text{CH}_3$ -functionalized surface at different pH (arrows indicate buffer rinsing).

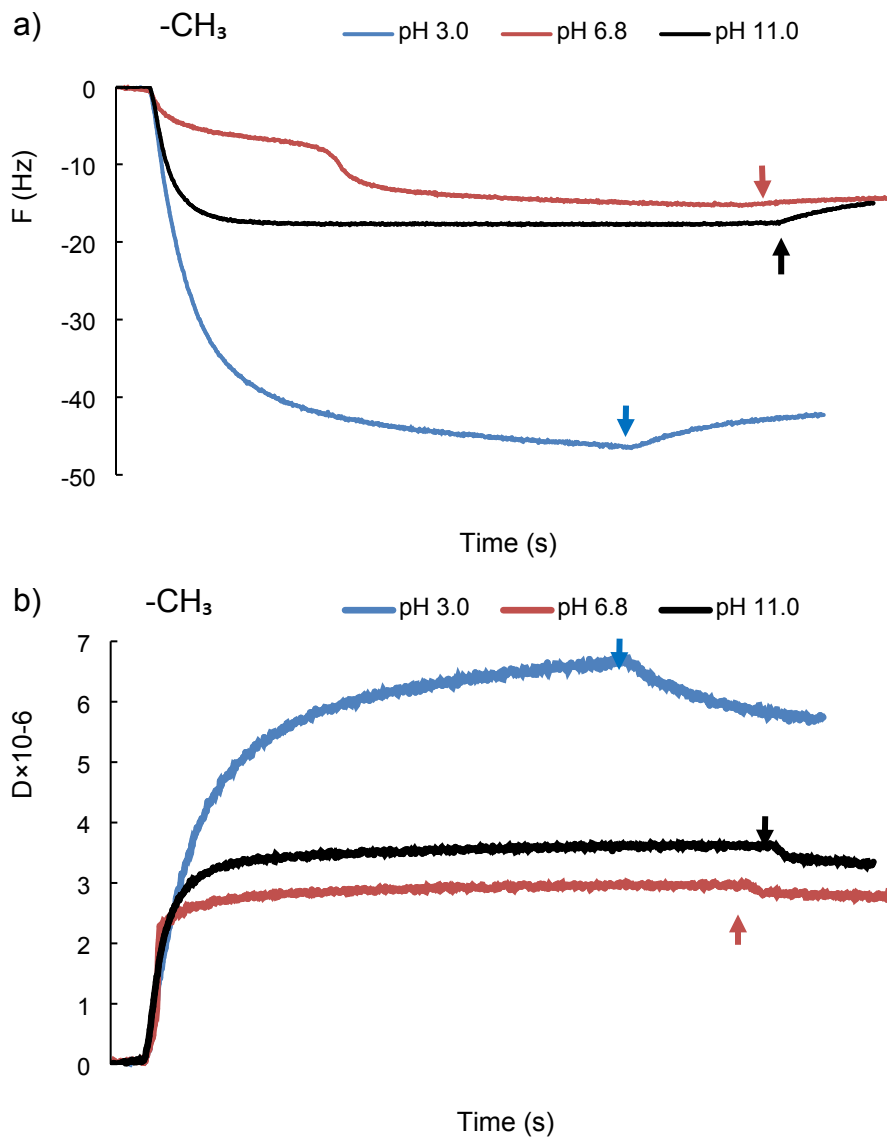


Figure S27. a) frequency b) dissipation changes of the 9th overtone of the adsorption of PVA-S polymer on the $-\text{CH}_3$ -functionalized surface at different pH (arrows indicate buffer rinsing).

Adsorption on $-\text{NH}_2$ -functionalized surface

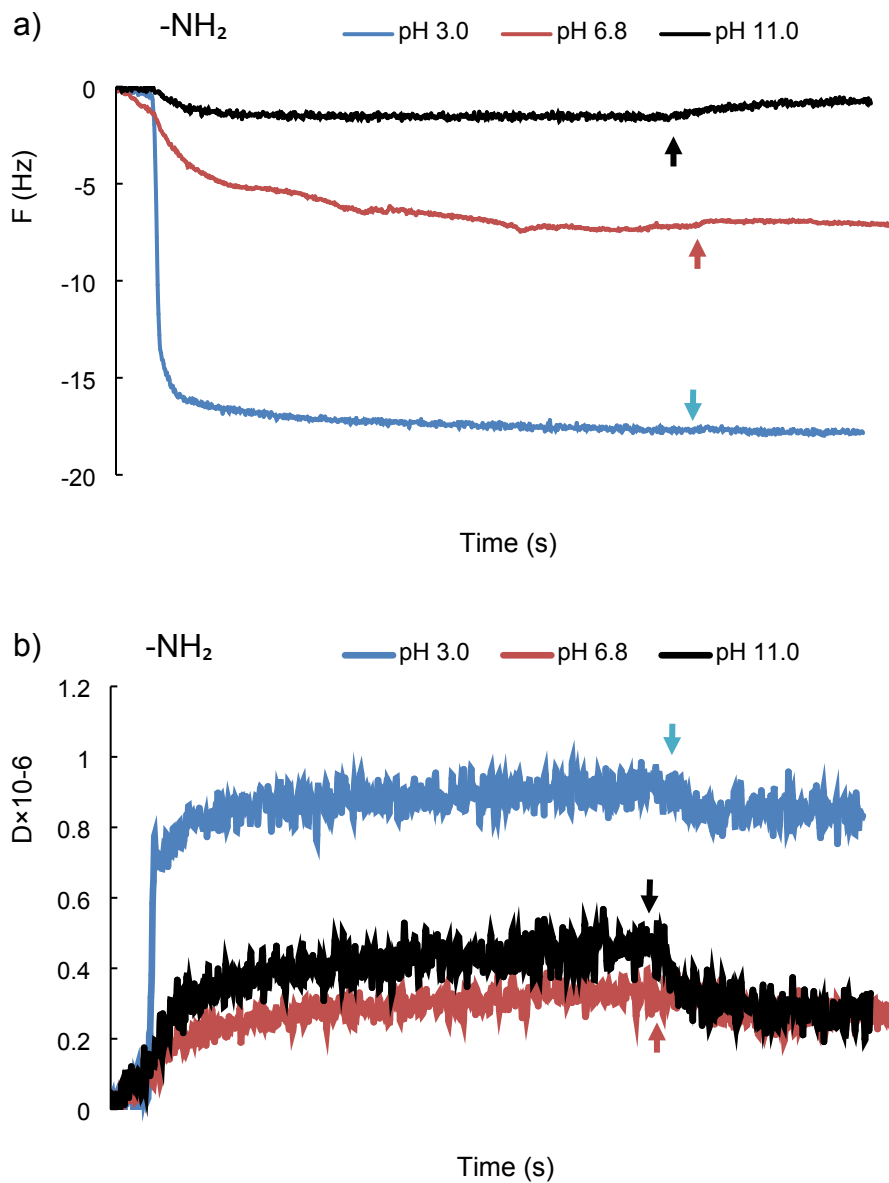


Figure S28. a) frequency b) dissipation changes of the 9th overtone of the adsorption of L-S polymer on the -NH₂-functionalized surface at different pH (arrows indicate buffer rinsing).

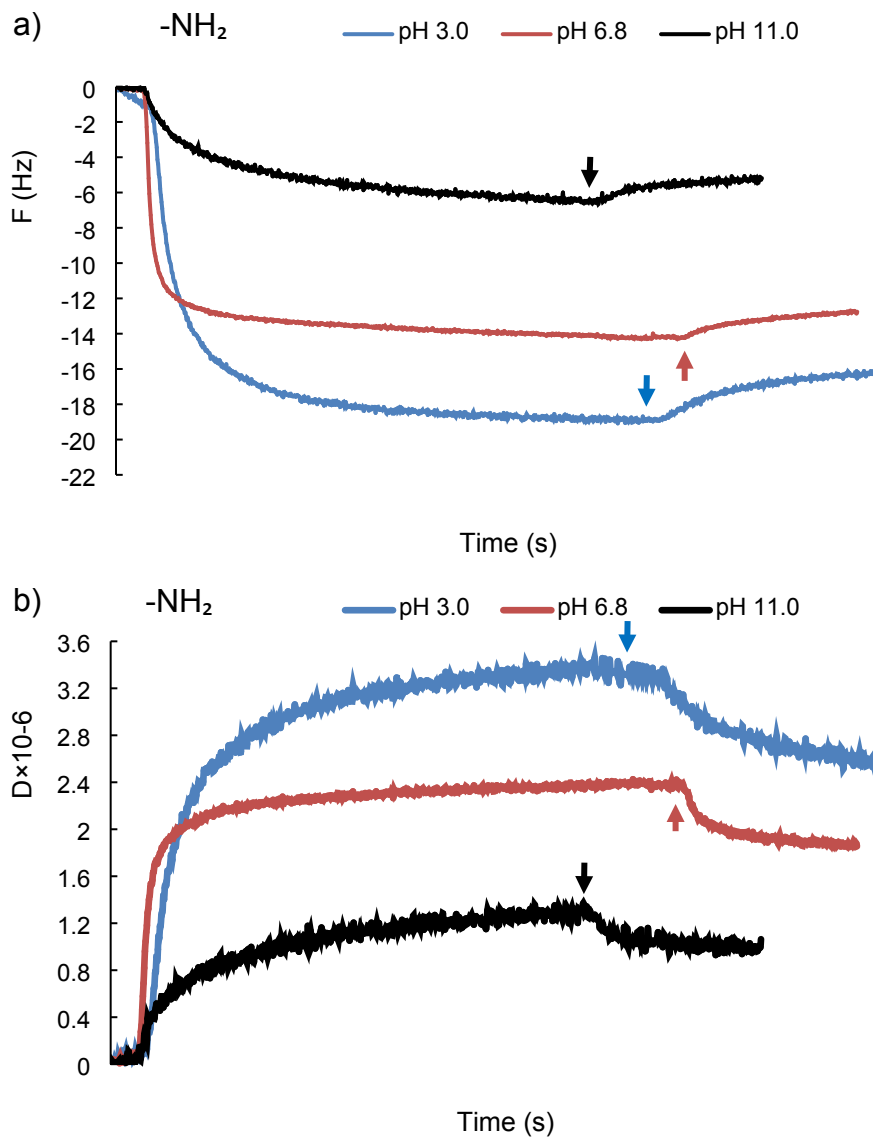


Figure S29. a) frequency b) dissipation changes of the 9th overtone of the adsorption of PVA-S polymer on the -NH₂-functionalized surface at different pH (arrows indicate buffer rinsing).

Effect of pH on the hydrodynamic radius (R_h) of L-S, and PVA-S

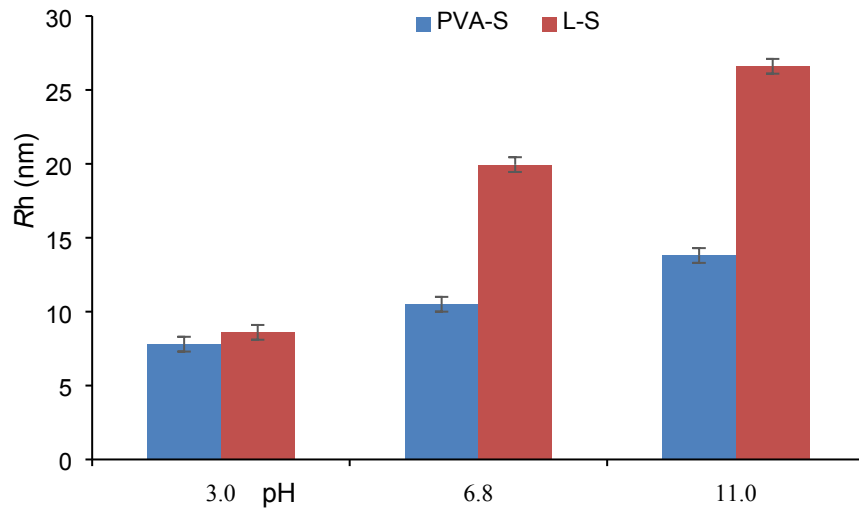
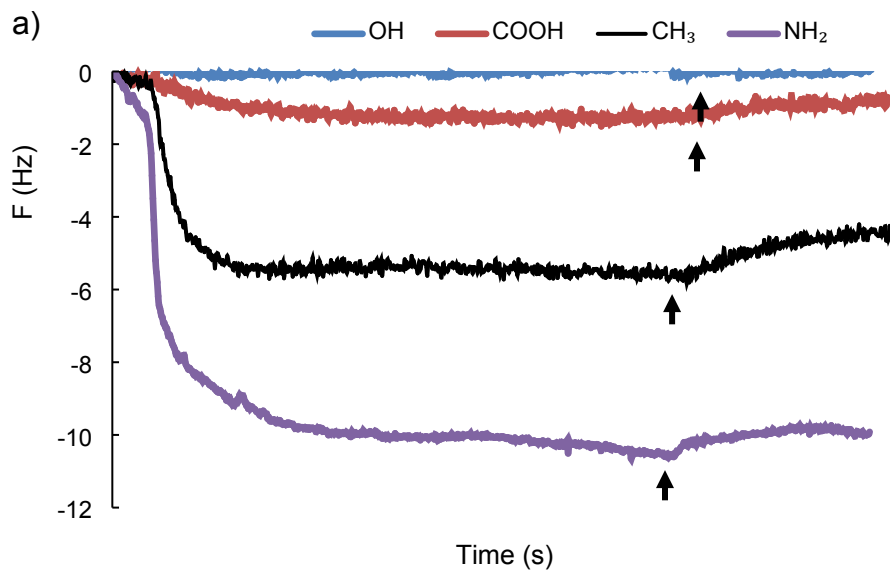
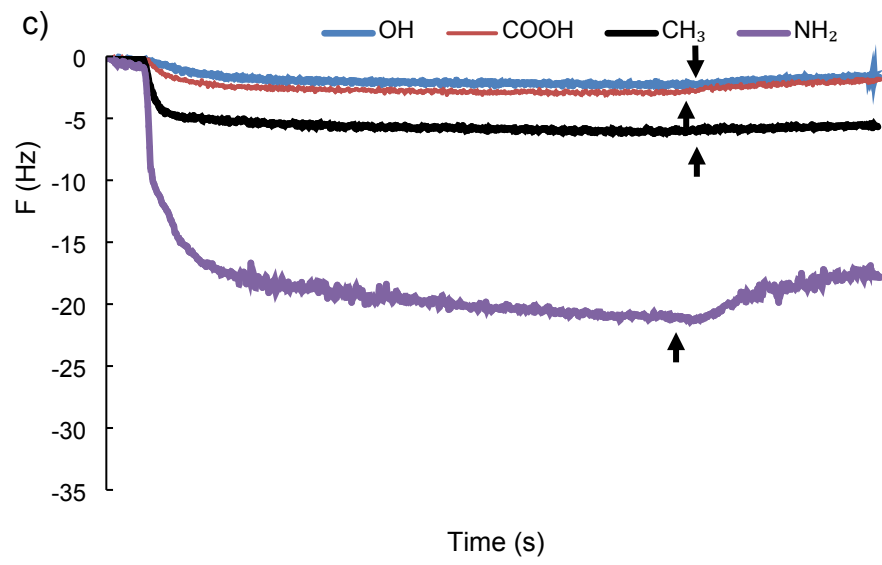
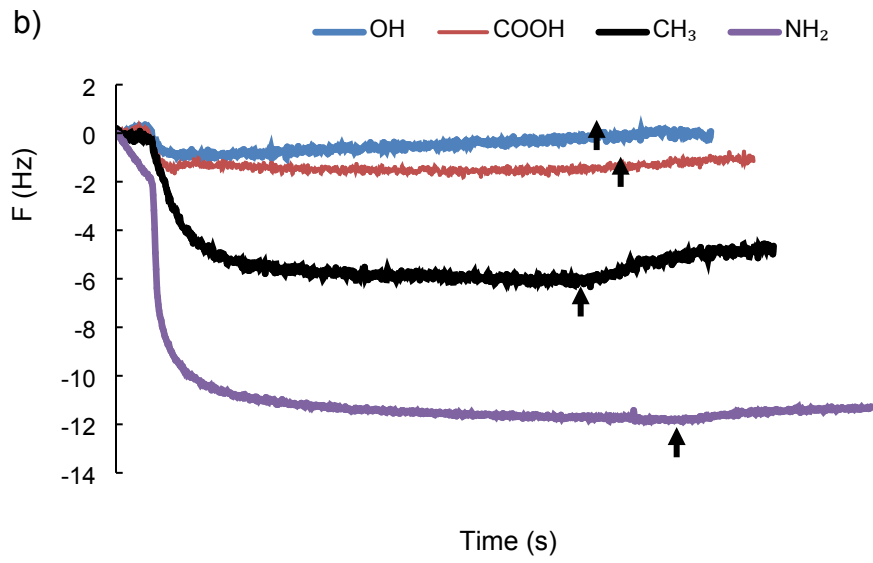


Figure S30. R_h as the function of pH for L-S, and PVA-S polymers

Effect of salt concentration on the adsorption of L-S and PVA-S on SAMs





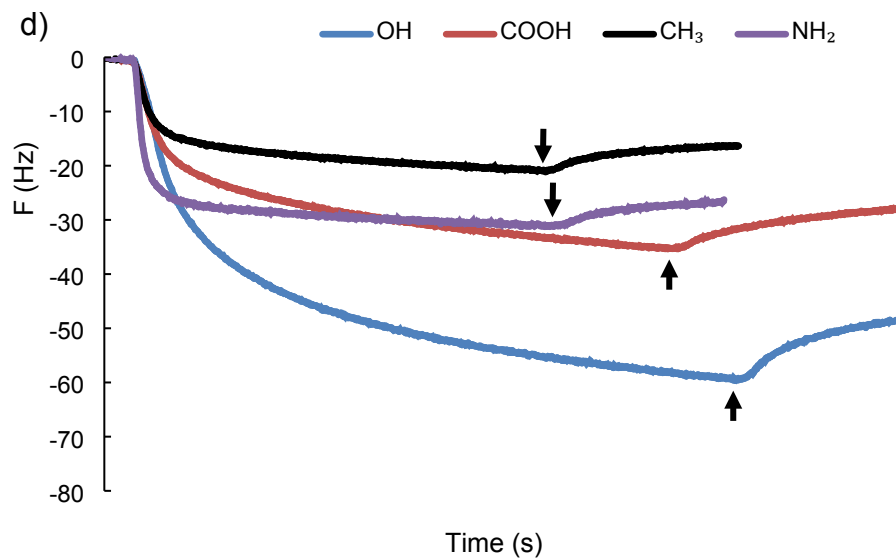
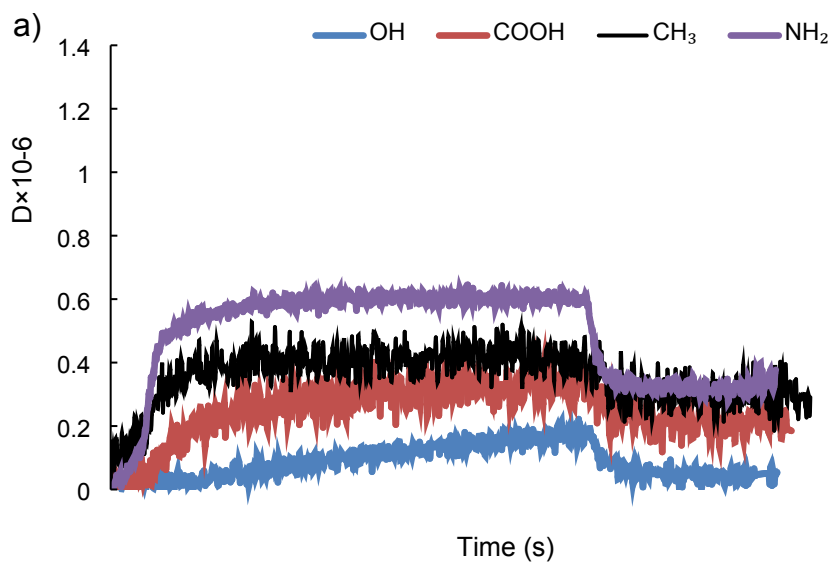
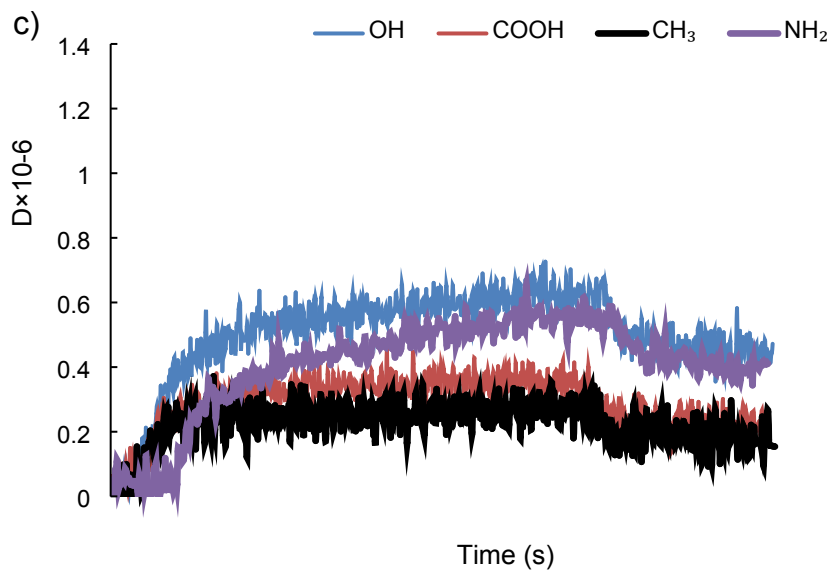
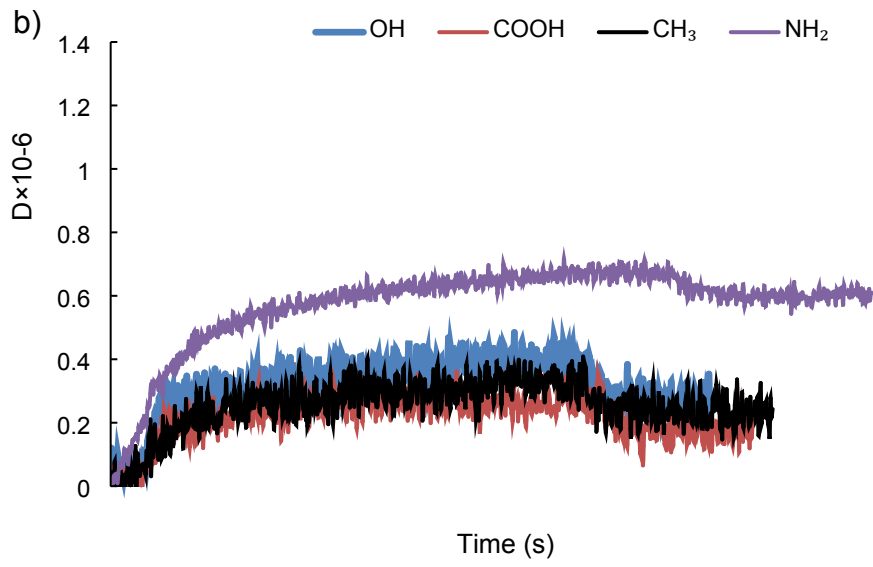


Figure S31. Frequency changes of L-S on SAMs of different chemistry at different salt concentrations of a) 1 mM, b) 10 mM, c) 100 mM, and d) 1000 mM (arrows indicate buffer rinsing).





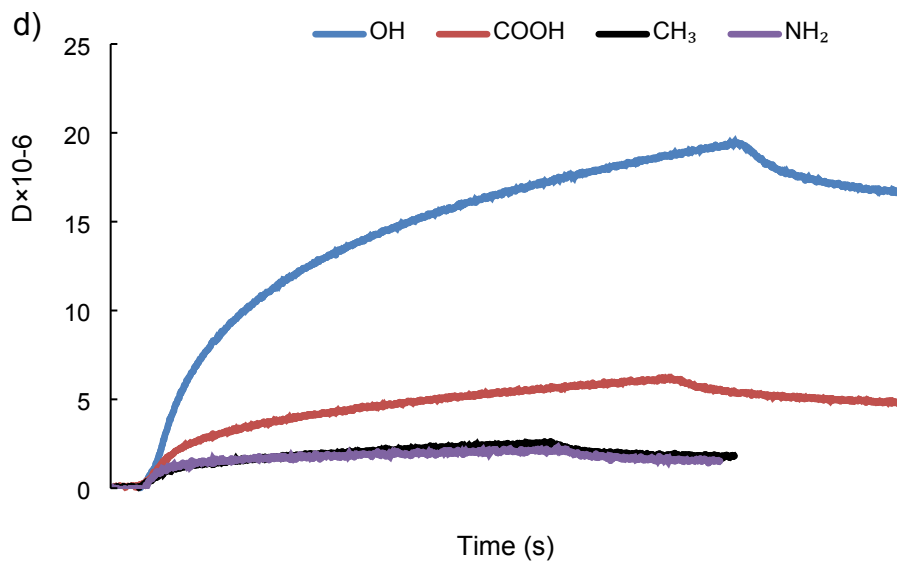
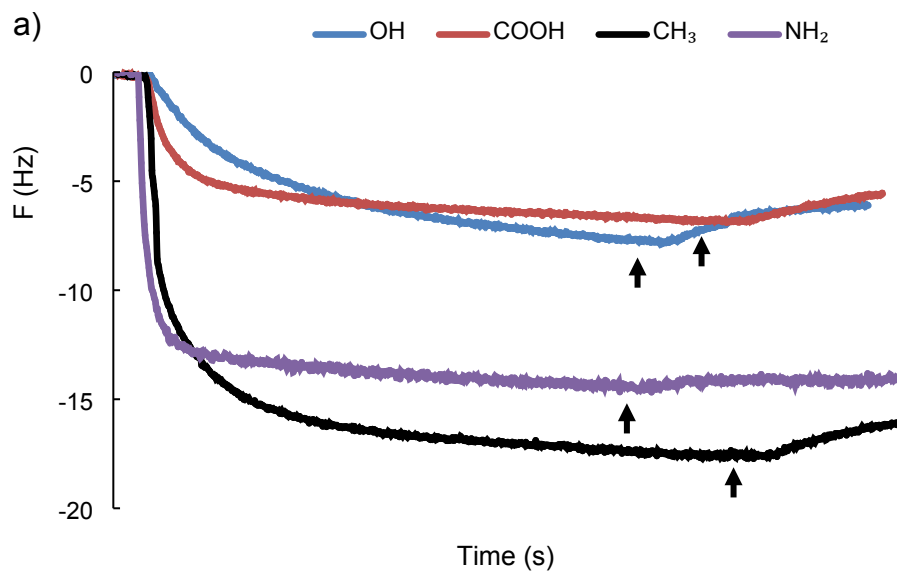
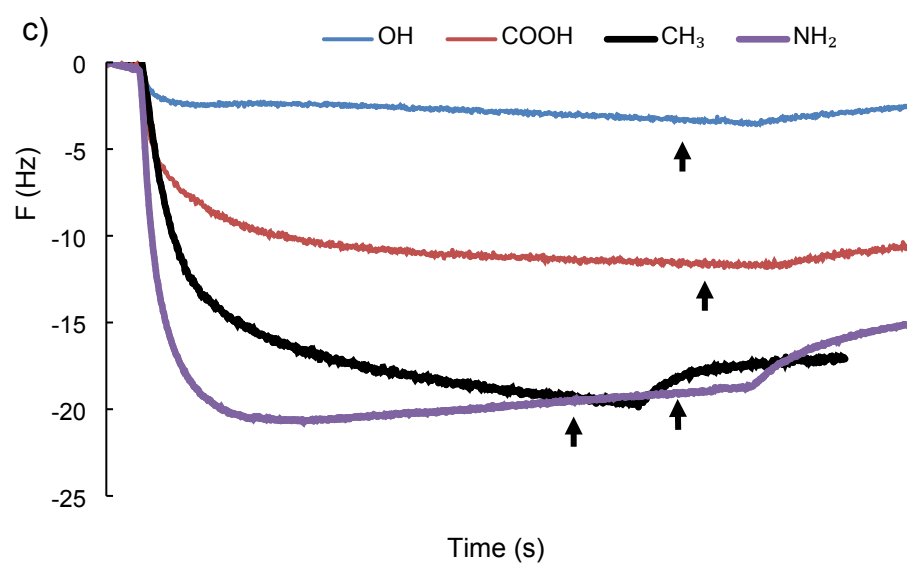
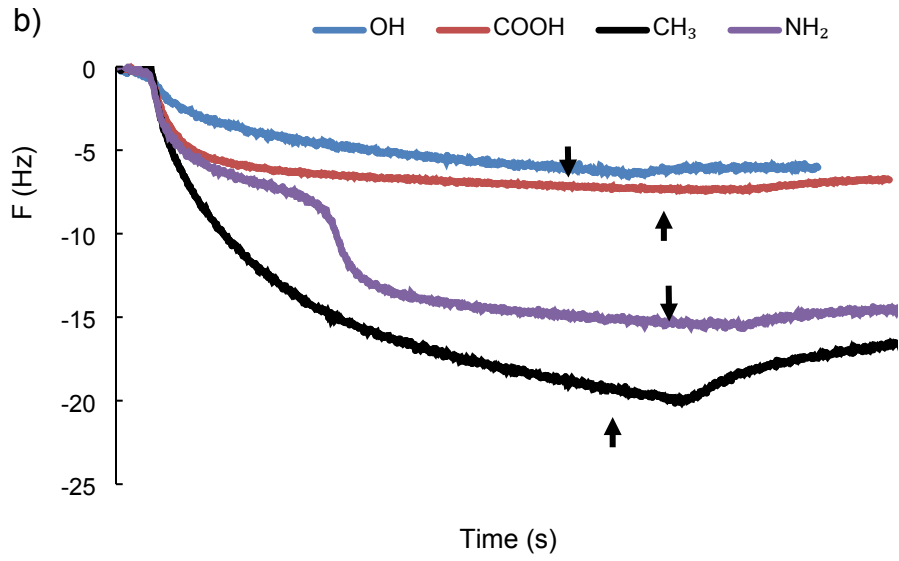


Figure S32. Dissipation changes of L-S on SAMs of different chemistry at different salt concentrations of a) 1 mM, b) 10 mM, c) 100 mM, and d) 1000 mM.





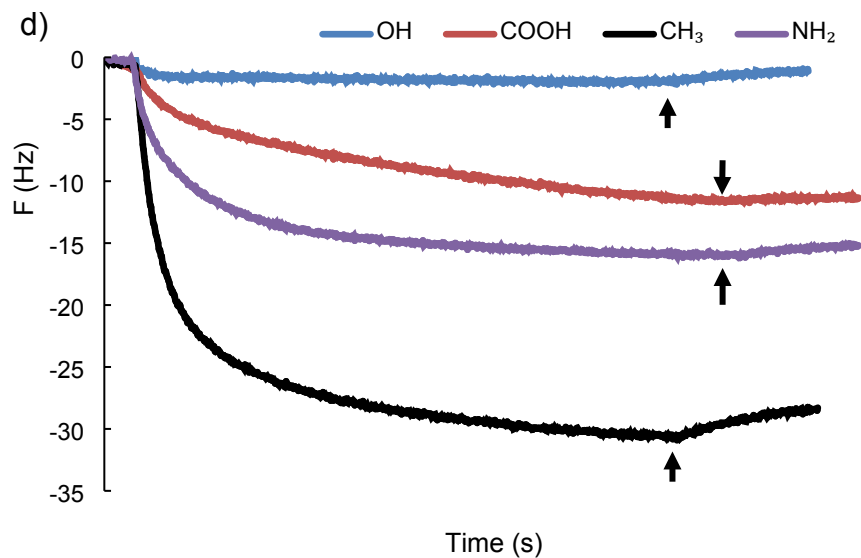
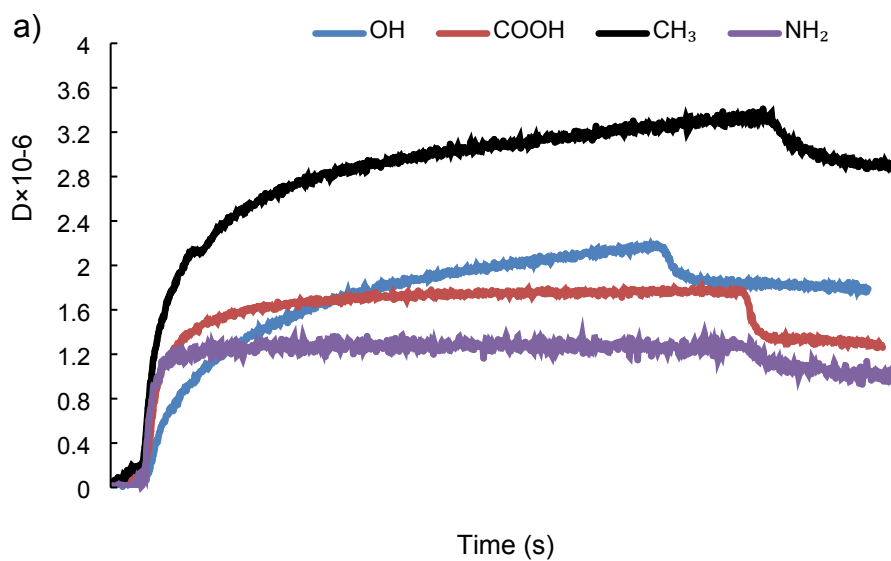
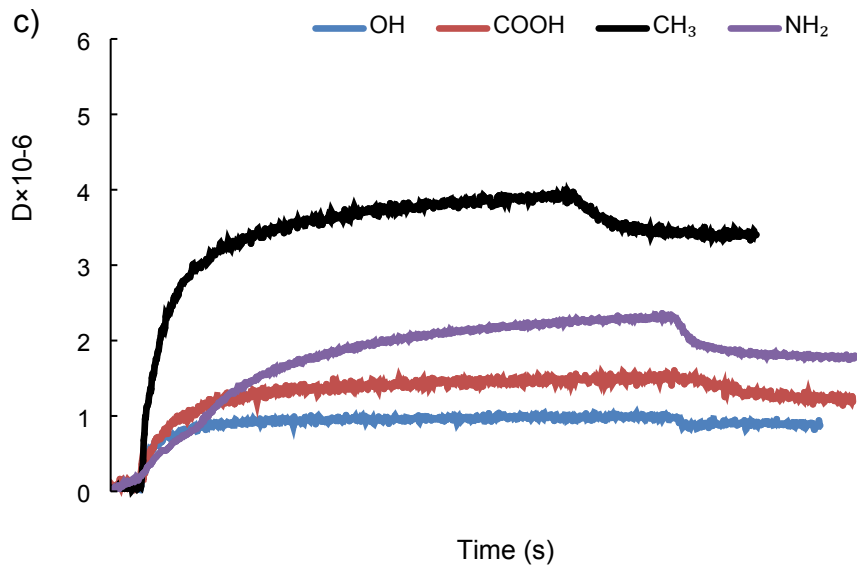
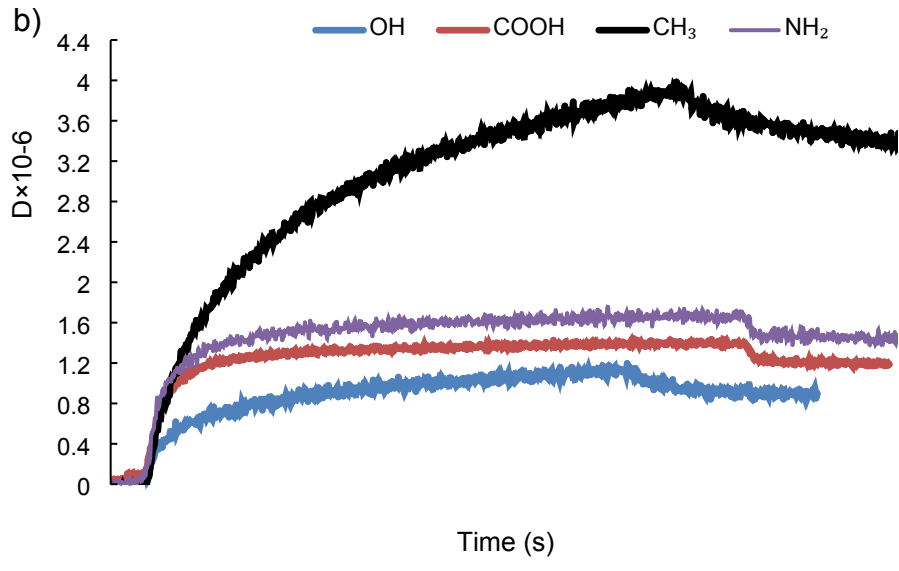


Figure S33. Frequency changes of PVA-S on SAMs of different chemistry at different salt concentrations of a) 1 mM, b) 10 mM, c) 100 mM, and d) 1000 mM (arrows indicate buffer rinsing).





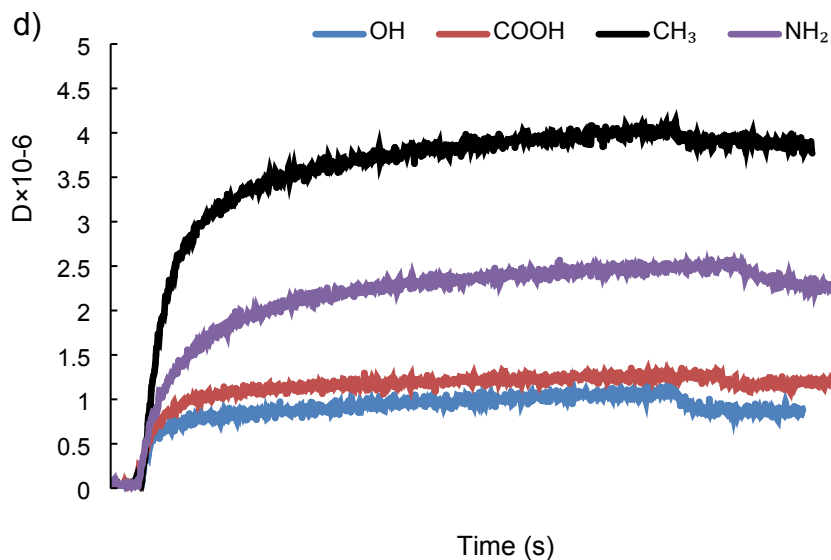


Figure S34. Dissipation changes of PVA-S on SAMs of different chemistry at different salt concentrations of a) 1 mM, b) 10 mM, c) 100 mM, and d) 1000 mM.

Effect of salt concentration on the hydrodynamic radius (R_h) of L-S, and PVA-S

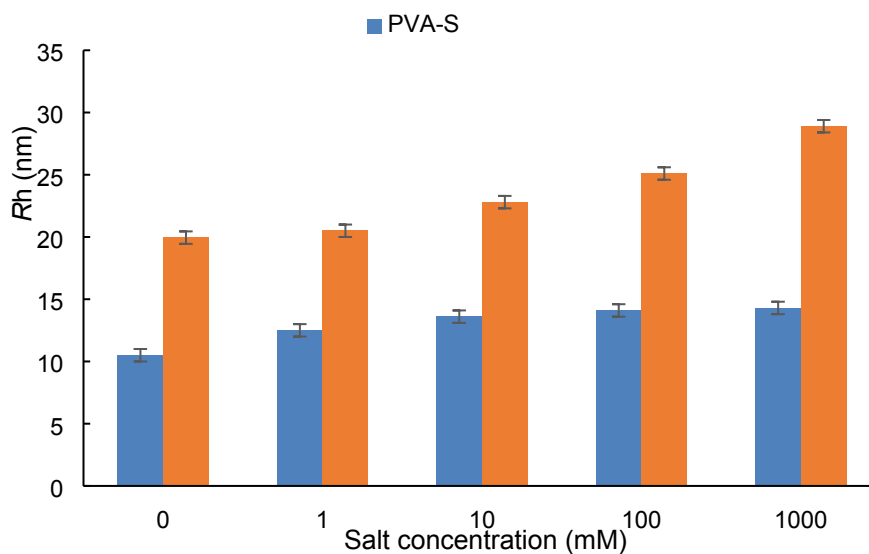


Figure S35. R_h as the function of salt concentration for L-S, and PVA-S polymers

References

1. C. J. Huang, F. S. Shieu, W. P. Hsieh and T. C. Chang, Acidic hydrolysis of a poly (vinyl acetate) matrix by the catalytic effect of Ag nanoparticles and the micellization of Ag-metal-containing polymer, *J. Appl. Polym. Sci.*, 2006, 100, 1457-1464.
2. A. E. Kazzaz and P. Fatehi, Fabrication of Amphoteric Lignin and its Hydrophilicity/Oleophilicity at Oil/Water Interface, *J. Colloid Interface Sci.*, 2020, 561, 231-243.
3. T. Rashid, C. F. Kait, I. Regupathi and T. Murugesan, Dissolution of kraft lignin using protic ionic liquids and characterization, *Ind. Crops Prod.*, 2016, 84, 284-293.
4. Y. C. Sun, J. L. Wen, F. Xu and R. C. Sun, Fractional and structural characterization of organosolv and alkaline lignins from *Tamarix austromongolica*, *Sci. Res. Essays*, 2010, 5, 3850-3864.
5. I. Korbag and S. Mohamed Saleh, Studies on the formation of intermolecular interactions and structural characterization of polyvinyl alcohol/lignin film, *Int. J. Environ. Stud.*, 2016, 73, 226-235.
6. F. Kong, K. Parhiala, S. Wang and P. Fatehi, Preparation of cationic softwood kraft lignin and its application in dye removal, *Eur. Polym. J.*, 2015, 67, 335-345.
7. N. E. El Mansouri and J. Salvado, Structural characterization of technical lignins for the production of adhesives: Application to lignosulfonate, kraft, soda-anthraquinone, organosolv and ethanol process lignins, *Ind. Crops Prod.*, 2006, 24, 8-16.
8. S. Zhou, L. Liu, B. Wang, F. Xu and R. Sun, Microwave-enhanced extraction of lignin from birch in formic acid: Structural characterization and antioxidant activity study, *Process Biochem.*, 2012, 47, 1799-1806.
9. A. Casas, M. V. Alonso, M. Oliet, E. Rojo and F. Rodríguez, FTIR analysis of lignin regenerated from *Pinus radiata* and *Eucalyptus globulus* woods dissolved in imidazolium-based ionic liquids, *J. Chem. Technol. Biotechnol.*, 2012, 87, 472-480.
10. M. Bouraada, M. S. Ouali and L. C. de Menorval, Dodecylsulfate and dodecylbenzenesulfonate intercalated hydrotalcites as adsorbent materials for the removal of BBR acid dye from aqueous solutions, *J. Saudi Chem. Soc.*, 2016, 20, 397-404.

11. C. A. Barbosa, P. M. Dias, A. M. D. C. Ferreira and V. R. Constantino, Mg-Al hydrotalcite-like compounds containing iron-phthalocyanine complex: effect of aluminum substitution on the complex adsorption features and catalytic activity, *Appl. Clay Sci.*, 2005, 28, 147-158.